Climate and ice sheet dynamics in Patagonia during the Last Glacial Maximum

Andrés Castillo-Llarena[1,2,*], Franco Retamal-Ramírez[3,4,5,*], Jorge Bernales[6], Martín Jacques-Coper[4,5,7], Matthias Prange[1], and Irina Rogozhina[2,8,9]

[1]MARUM - Center for Marine Environmental Sciences and Faculty of Geosciences, University of Bremen, Bremen, Germany
[2]Department of Geography, Norwegian University of Science and Technology, Trondheim, Norway
[3]Centro de Investigación Gaia Antártica, Universidad de Magallanes, Punta Arenas, Chile
[4]Departamento de Geofísica, Universidad de Concepción, Concepción, Chile
[5]Center for Climate and Resilience Research (CR)2, Universidad de Concepción, Concepción, Chile
[6]Institute for Marine and Atmospheric Research Utrecht, Utrecht University, Utrecht, Netherlands
[7]Center for Oceanographic Research COPAS COASTAL, Universidad de Concepción, Concepción, Chile
[8]Centro de Estudios Avanzados en Zonas Áridas (CEAZA), La Serena, Chile
[9]Departamento de Ciencias de la Tierra, Universidad de Concepción, Concepción, Chile
[*]These authors contributed equally to this work.

Correspondence: Andrés Castillo-Llarena (acastillollarena@marum.de) and Franco Retamal-Ramírez (fretamal@umag.cl)

Abstract. During the Last Glacial Maximum (LGM, ~ 23,000 to 19,000 years ago), the Patagonian Ice Sheet (PIS) covered the central chain of the Andes between ~ 38° S to 55° S. Existing paleoclimatic evidence ~~– mostly –~~mostly derived from glacial ~~landforms –~~landforms~~–~~ suggests that maximum ice sheet expansions in the Southern and Northern Hemispheres were not synchronized. However, large uncertainties still exist in the timing of the onset of regional deglaciation as well as its major drivers. Here we present an ensemble of numerical simulations of the PIS during the LGM. ~~Our aim is to assess the ability~~ We assess the skill of paleoclimate model products ~~to reproduce~~ in reproducing the range of atmospheric conditions needed to enable ~~the~~ an ice sheet growth in concordance with geomorphological and geochronological evidence. The resulting ~~ensemble is then used as a guideline for the evaluation of the PMIP3 and PMIP4 model performance across different sectors of the former PIS~~best-fitted climate product is then applied as forcing in transient simulations during the last 70 ka using a glacial index approach based on offshore records and Antarctic ice cores. Our analysis suggests a strong dependence of the PIS geometry on near-surface air temperature forcing. ~~All the ensemble members driven by PMIP products are not able to reproduce the reconstructed~~ Most ensemble members underestimate the ice cover in the northern part of Patagonia~~. In contrast, the modelled PIS tends~~, while tending to expand beyond its constrained boundaries in south-eastern Patagonia. We largely attribute these discrepancies between the model-based ice geometries and geological evidence to the low resolution of paleoclimate models and their prescribed ice mask. We conclude that among all tested climate ~~forcings, the PMIP4 climate models INM-CM4-8 and~~ products, the forcing data from the MPI-ESM1-2-LR ~~produce the necessary~~ model produces conditions for ice sheet growth across Patagonia ~~. It should be kept in mind that this analysis is based only on the evaluation of the modelled ice sheet extent because geological constraints on~~ that best align with the available evidence. Our transient simulations reveal that the ~~former ice thickness are still lacking. Nevertheless, our analysis suggests that a realistic PIS geometry at the LGM can be reproduced only if the complex topographic features of the Andes are properly resolved by climate models~~distinct local glacial peak in

Patagonia leave a discernible mark on off-shore records along the region. In the southernmost sector, evidence suggests full glacial conditions during Marine Isotope Stage 3 (MIS3), succeeded by a warming trend towards MIS2. However, in northern Patagonia, this deglacial trend is absent, indicating a relatively consistent signal throughout MIS3 and MIS2. Notably, Antarctic cores do not reflect a glacial history consistent with the geochronological observations. Therefore, investigations of the glacial history of the PIS should take into account southern midlatitudes records to capture effectively its past climatic variability.

1 Introduction

At present, there are only two ice sheets on Earth. The Antarctic ice Sheet is the largest, with an ice volume of 26.04 $\pm$ 0.4 $\times 10^6$ km^3 that can be translated into a sea-level equivalent (SLE) of 57.0 $\pm$ 0.9 m (Morlighem et al., 2020). The Greenland Ice Sheet contains 2.99 $\pm$ 0.2 $\times 10^6$ km^3 of ice, which ~~is equivalent~~ corresponds to a SLE of 7.42 $\pm$ 0.05 m (Morlighem et al., 2017). However, during the last glacial period, especially during the global Last Glacial Maximum (LGM, 23,000 to 19,000 years before present, ka), much of North America was buried under the North American Ice Sheet complex, the Eurasian Ice Sheet complex stretched across most of Northern Europe, and the Patagonian Ice Sheet (PIS) covered the western part of southern South America. ~~Together,~~ The ice locked away in these former ice sheets represented a SLE of around 113.9 m (Simms et al., 2019)~~and, consequently, global sea level dropped to~~ . When the contributions from Antarctica and Greenland are added on top, this results in an estimated total sea-level drop at of 120-134 m below present between 29 and 21 ka (Lambeck et al., 2014). ~~As such, this~~ This period was marked by partly exposed continental shelves, strong winds, dry conditions, and a total greenhouse gas concentration lower than during the Pre-Industrial (PI; Monnin et al., 2001; Bartlein et al., 2011; Kohfeld et al., 2013; Simms et al., 2019)~~. The latter triggered a~~ ; lowering of the global mean ~~air temperature, with current estimates of the LGM-PI global surface air (negative) temperature anomaly ranging from~~ surface air temperature by 3.2 °C to 6.7 °C with respect to the pre-industrial level (Schneider von Deimling et al., 2006; Holden et al., 2010; Annan and Hargreaves, 2013; Tierney et al., 2020; Kageyama et al., 2021).

The PIS was ~~relatively a~~ a relatively small ice sheet, comparable in size to the former Celtic Ice Sheet that covered the British Isles during the LGM (Hughes et al., 2016). ~~At present, its~~ Its former evolution is still subject to considerable uncertainties regarding ~~its past extents, volumes, and relative contributions~~ ice extent, ice volume, and contribution to sea level variations, mainly due to the scarcity of ~~solid geological evidence~~ geological evidence (Hulton et al., 2002; Davies et al., 2020; Wolff et al., 2023) . Only recently, Davies et al. (2020) succeeded in building a geochronological data set of a reasonable size and robustness, arriving at the conclusion that the PIS reached its maximum extent during the Marine Isotope Stage (MIS) 3 at $\sim$ 35 ka. This state remained nearly unchanged until 27 ka, which is much earlier than the global timing estimates for LGM. This is a generic estimate because the evidence suggests that the timing of its maximum extent changed with latitude: the northern sector located between of 38° S to 48° S is thought to have reached its largest area between 33 to 28 ka, while its southern counterpart (between 48° S to 56° S) peaked much earlier, at around 47 ka. Based on simplifying assumptions, Davies et al. (2020) estimated a uniform maximum PIS extent of 492,600 km^2 at 35 ka, corresponding to a SLE of around 1.5 m.~~To date, the most common way to define the LGM is through a globally integrated ice volume, zooming in on the global climate that was closest~~

to equilibrium during the last glacial period. However, this is a limiting assumption: during the last glacial period, many of the then-existing ice sheets seem to have reached their maximum extent at different dates (Hughes et al., 2013), with both the ice masses and the climate broadly in equilibrium.

Studies of past climate conditions commonly rely on global climate models validated and calibrated against paleoclimate proxy data (Braconnot et al., 2012; Annan and Hargreaves, 2013; Evans et al., 2013). This combination of models and observations is a fundamental tool for understanding how Earth's climate has responded to changes in external (e.g. orbit, insolation) and internal (e.g. greenhouse gases) conditions on global and regional scales. When coupled to large water reservoirs, such as the ocean and ice sheets, these models can provide important insights into the role of climate-ocean-ice feedbacks (e.g. albedo, freshwater influx) that can have long response times. To better understand the results from these models, the Paleoclimate Modelling Intercomparison Project (PMIP) has focused exclusively on paleoclimate reconstructions, aiming to provide an effective mechanism for standardising and coordinating paleoclimate modelling experiments among research groups across the globe (Meinshausen et al., 2011). During the different stages of PMIP (1-4), paleo experiments have been performed with prescribed forcings, including orbital parameters, sea level, topography (including ice sheet elevations), and greenhouse gas concentrations (Joussaume and Taylor, 1995; Braconnot et al., 2007; Harrison et al., 2015; Kageyama et al., 2017).Recently, Yan et al. (2022) modelled the PIS extent during the LGM combining present-day climatology and PMIP outputs the temperature and precipitation from 21 PMIP outputs from phases 2, 3 and 4, to analyse the degree of agreement between their modelled geometries and the PATICE reconstruction (Davies et al., 2020). One of the main findings of their study is that most of the uncertainty in the modelled PIS geometry is associated with the PMIP forcing, producing an overestimation of the ice-covered extent over vast regions, while showcasing an underestimation of ice in other areas. These results reflect the inability of PMIP3 most PMIP model products to provide climate conditions that allow for ice sheet advance in the northernmost sectors of Patagonia during the LGM, even under a somewhat extreme choice of model parameters. In contrast, Only some of the PMIP4 models seem to present the climate conditions needed to trigger ice sheet inception and growth in this region. However, Yan et al. (2022) did not provide potential reasons for these discrepancies.

In a much earlier study, Hulton et al. (2002) used numerical modelling to show that a drop in present-day temperatures of at least 6 and modified wind patterns (decreasing wind intensity at ~ 50° S where the core of the westerlies is concentrated and increasing them in other latitudes) were a prerequisite for PIS inception. This is because present-day precipitation rates are very high in southern Patagonia and very low in northern Patagonia, compared to a more even distribution during the LGM (Kohfeld et al., 2013).In this study, we use the numerical ice sheet model SICOPOLIS (Greve, 1997; Sato and Greve, 2012) to explore the range of climate conditions that leads to a good match between the modelled PIS and field-derived geometries . during the global LGM. The resulting best-fitted climate model is then used to perform transient simulations throughout the MIS4 and MIS2 to explore the timing of the local maximum ice extension and the consequent deglaciation. Our ice sheet modelling experiments are driven by climate products from phases 3 and 4 of PMIP and employ the glacial index method derived from off-shore records and Antarctic cores. Furthermore, we assess the relative performance of LGM climate forcings in different sectors of the former ice sheet our simulations against the geochronological reconstruction of Davies et al. (2020). Finally, we investigate potential reasons for their different performance throughout Patagonia. Present-day topographic map of

Patagonia based on ETOPO1 (Amante and Eakins, 2009). Present-day ice fields are indicated and correspond to the Northern Patagonian Icefield (NPI), Southern Patagonian Icefield (SPI) and Cordillera Darwin Icefield (CDI). PIS reconstruction of (Davies et al., 2020) for 20 . LGM coastal lines marking lower sea level (-120 m) are shown in dark turquoise contour.

2 Methods

2.1 Model set-up

Our PIS simulations All numerical simulations of the PIS in this study are performed using the open source, three-dimensional, thermomechanical ice sheet model SICOPOLIS (SImulation COde for POLythermal Ice Sheets; Greve, 1997; Sato and Greve, 2012) and cover the area between 80° W and 62° W and between 36° S and 58° S (Fig. ??)and are performed using the open source, three-dimensional, thermomechanical polythermal ice sheet model SICOPOLIS (SImulation COde for POLythermal Ice Sheets)version 5.2 (Greve, 1997; Sato and Greve, 2012). Experiments are designed with an 1). This model domain is discretised using an equidistant grid with a horizontal resolution that ranges between 4 and 8 horizontal resolution and 81 vertical grid pointskm, for equilibrium and transient simulations, respectively (see Sections 2.2 and 2.3). In the vertical dimension, the grid is extruded into 81 terrain-following layers that densify towards the base, from which 3 are allocated to accommodate the potential presence of temperate ice. Within this three-dimensional grid, the temperate ice layer if it exists. In addition, 41 gridpoints are reserved for the bedrock, where geothermal flux towards the ice sheet bed is prescribed at the bottom of the bedrock layer.The model combines the shallow-ice approximation (SIA) and shelfy-stream approximation (SStA) in order to reproduce the entire range of ice flowing conditions across an ice sheet (Bernales et al., 2017). The time step for the calculations of ice velocity , topography changes, internal ice temperature, water content, and age of ice is set to model discretises and approximates the Stoke equations for ice velocities using a combination of the shallow ice and shelfy stream approximations (SIA and SStA, respectively) following the hybrid approach of Bueler and Brown (2009), as described in Bernales et al. (2017). This hybrid model solves for an ice velocity field that corresponds to a given ice geometry, mass balance, and thermal state. The resulting velocity field is then used to compute the evolution of ice within the domain by integrating the model forward in time under a time step that ranges between 1 year.and 0.5 years, depending on the horizontal grid resolution applied.

At the beginning of each simulation, an ice-free topography is prescribed from the and mapped onto the horizontal model grid based on the ETOPO1 data set (Amante and Eakins, 2009). This initialisation assumes a global sea level drop of 120 , based on reconstructions for the LGM (Lambeck et al., 2014), which is applied homogeneously over the entire model domain. We use Within this bedrock, a lithospheric model layer is represented by an extension of the extruded horizontal grid spanning 41 additional vertical points. At the base of this layer, a constant, spatially homogeneous value of 100 for the geothermal heat flux , in of 100 $\mathrm{mW\ m^{-2}}$ is applied —in agreement with averaged values observed in Patagonia (Hamza and Vieira, 2018)—, which serves as the lower thermodynamical boundary condition for the model. Glacial isostatic adjustment of this bedrock produced by temporal variations of the ice mass load is accounted for through an elastic-lithosphere, relaxing-asthenosphere model (ELRA) , in which the effects of ice loading and unloading on the planet's surface are parameterised through a

~~constant relaxation time (e.g., Greve and Blatter, 2009).~~ model (e.g., Greve and Blatter, 2009) using standard parameter values (see Table 1).

~~The~~ This initialisation assumes a global sea level drop of 120 m, based on reconstructions for the LGM (Lambeck et al., 2014), which is applied homogeneously over the entire model domain. The ice is only allowed to advance on land, being immediately calved out on the coast. Ocean temperature and dynamics beyond the sea level change have no implication whatsoever in our simulations.

The inception and evolution of the PIS in our model is driven by the surface mass balance (SMB), which is calculated as the difference between ~~ice accumulation and~~ applied fields of accumulated precipitation and surface ablation. The latter is computed using a positive-degree-day (PDD) model ~~(Calov and Greve, 2005). Accumulation depends on~~ following Calov and Greve (2005), based on a given near-surface air temperature field and the parameters in Table 1. PDD values have been selected based on contemporary and paleo studies in the area (Fernández and Mark, 2016; Yan et al., 2022; Cuzzone et al., 2023). Surface mass accumulation is assumed to depend on monthly precipitation and temperature fields, such that the transition between solid and liquid precipitation is linearly proportional to variations in air temperature (Marsiat, 1994). Here we use a transition range of 0 °C to 2 °C, producing purely solid or purely liquid precipitation below or above this temperature range, respectively. ~~To account for the~~ As the model domain surface evolves due to the advance and retreat of the PIS during a simulation, discrepancies between the ~~topographies in climate and ice sheet models,~~ prescribed (fixed) topography used in the PMIP climate model snapshots and the dynamic one in SICOPOLIS are accounted for by implementing a near-surface ~~air temperatures are corrected using a lapse rate~~ air temperature lapse-rate correction of -6.5 K km^{-1}. ~~At the coasts, where the ice might become afloat, calving at the front of ice shelves is parameterised through an instantaneous calving of ice-filled model cells whose ice thickness becomes thinner than 50 . General model parameter values used in the ice sheet simulations are summarised in Table 1~~The precipitation has been reduced as function of the temperature (Huybrechts, 2002). The resulting atmospheric temperatures near the surface of the ice are then applied as the upper thermodynamical boundary conditions. ~~Description of the most important parameters in the model set-up. Model component Description Value Units Ice rheology Ice density 910.00 Gravity acceleration 9.81 Glen's flow law exponent 3.00 - Ice specific heat capacity 4170.00 Ice thermal conductivity 2.10 Water latent heat of fusion 3.34×10^5 Enhancement factor for the SIA and SSA 1, 0.5 - Bedrock Geothermal heat flux 100.00 Lithosphere density 3300.00 Sea level -120.00 Surface and atmosphere PDD standard deviation 3 Temperature of snow precipitation 0 Temperature of rain precipitation 2 Degree day factor for snow 8 Degree day factor for ice 3~~

2.2 ~~Climate forcing and experimental design~~

~~We generate a range of PIS geometries by forcing the ice sheet model with atmospheric products from several~~

2.2 Equilibrium simulations at the global LGM

Starting from the ice-free conditions described in Section 2.1, an ensemble of model simulations is run forward in time, each member forced by a different pair of matching near-surface air temperatures and total precipitation fields from 15 climate models that participated in the LGM experiments during phases 3 and 4 of PMIP. ~~Then, we evaluate the resulting geometries against~~

the corresponding time-snapshot at A list of these climate models is presented in Table 2. The forcing fields contained in a given LGM climate snapshot are applied in a constant manner, i.e., without any temporal variations as the domain evolves, except for the lapse-rate correction and elevation desertification described in Section 2.1. In areas where a temperature-precipitation pair results in a positive SMB, inception of ice will occur. The ice mass will then grow and advect outwards, leading to an advance of the emerging PIS. The extent of this advance will be limited by areas where a negative SMB fully compensates for the advected ice from upstream. As the PIS thickens, the amount of ice transported downstream increases, while surface ablation decreases due to the cooling of near-surface temperatures as a result of the lapse-rate correction. This positive feedback is then balanced by a reduction in the available precipitation as elevation desertification sets in. As the model is integrated forward in time, these competing effects shape the advancing PIS until a balance between the accumulation and ablation zones of the entire ice sheet is reached. Each equilibrium simulation in this study spans 10,000 model-years, which is enough to bring the domain to a steady state under each of the time-invariant climate conditions. The resulting PIS geometry for each of the ensemble members is evaluated against the LGM snapshot (20 ka) from the PATICE geological reconstruction (Davies et al., 2020) . Near-surface air temperature and precipitation from thirteen climate models (see Table 2)were used to compute anomalies as the difference (for temperatures) or ratio (for precipitation) between their respective LGM and PI climate snapshots, separately for each climate model. The monthly mean LGM-PI temperature differences are added to the present-day climate from ERA 5, averaged over the period 1979-2020. The monthly mean present-day precipitation fields are multiplied by their corresponding monthly mean LGM/PI precipitation ratios (instead of differences) to prevent negative values . Using the resulting ensemble of precipitation and near-surface temperature pairs as forcing, each ice sheet model simulation is then run for 10, 000 model years, which is enough to reach an equilibrium with these time-invariant climate conditions. in Section 3.

PMIP3 and PMIP4 models analysed in the present study. Model name PMIP phase Atmospheric model resolution

2.3 Transient simulations through the MIS3 and MIS2

The equilibrium simulations described in Section 2.2 assume constant, peak glacial conditions from PIS inception to steady-state. These assumptions introduce a cold bias both in the internal thermal regime of the ice sheet and in the applied SMB. For the former, the influence of warmer or colder past climates on englacial conditions can last for tens of thousands of years after such conditions have disappeared, given the slow response time-scales of ice sheets (Rogozhina et al., 2011).

CCSM4 III 1.25 x 0.9 CNRM-CM5 III 1.4 x 1.4 COSMOS-ASO III 3.8 x 3.7 FGOALS-g2 III 2.8 x 3-6 GISS-E2-R III 2.5 x 2.0 IPSL-CM5A-LR III 3.8 x 1.9 MIROC-ESM III 2.8 x 2.8 MPI-ESM-P III 1.88 x 1.9 MRI-CGCM3 III 1.18 x 1.1 INM-CM4 IV 1.5 x 2.0 MPI-ESM1-2-LR IV 1.88 x 1.88 MIROC-ES2L IV 2.8 x 2.8 AWI-ESM-1-1-LR IV 1.88 x 1.88 With the aim of reducing the biases mentioned above and explore the glacial history of the PIS before the global LGM, we perform a second ensemble of simulations using transient climate forcing. This forcing is derived by first selecting a well-performing member from the equilibrium ensemble of simulations (see Section 3). Then, the LGM climate snapshot from the same climate model is complemented by a corresponding PI snapshot, representing peak glacial and interglacial conditions, respectively. In order to generate a climate state at any given model time, these two snapshots are then subjected to a weighted interpolation following a glacial index (henceforth GI) approach (e.g., Mas e Braga et al., 2021). Here, the time-dependent weight is in turn derived from

a list of ice and offshore sediment cores (see Table 3). For all core records, the computation of the GI uses the 19-23 ka mean of either d18O (for ice cores) or sea-surface temperature (SST; for sediment cores) to define peak glacial conditions. Likewise, peak interglacial conditions are defined against a near-PI period by averaging over the last 3 ka. The latter is, however, not possible for the GeoB3327-5 and PS75/034-2 sediments cores, which lack late Holocene data. For these two cores, values from the centennial time-scale SST reconstruction COBEV2 (Ishii et al., 2005) have been used to fill the data gap. With this range of far- and near-field core locations, we investigate whether the offshore records along the Pacific margin contain any imprints of an earlier, local glacial maximum in the Patagonian region. Each of the simulations in the transient ensemble is initialised from ice-free conditions and keeping the setup of the equilibrium ensemble as described in Section 2.2, except for the climate forcing. Then, each member is run under a different record-derived GI spanning the period between 70 ka and PI, encompassing both the MIS 3 and 2.

3 Results

~~Our~~

3.1 Performance of the PMIP models at the LGM in Patagonia

Our equilibrium model experiments produce a wide range of PIS geometries, some of which are generally comparable with the geologically constrained ice extents, while others yield considerably reduced and/or overextended ice cover (Fig. ~~??~~4). We have divided the former PIS extent into 3 distinct latitudinal ranges based on their model sensitivity and response to the imposed climate. Each of these areas is described and analysed in detail in the following sections. First, south of 52° S, most ensemble members exhibit an unrealistic build-up of ice in south-eastern Patagonia, with a much larger ice-covered area than inferred from the geological evidence. Second, between 44° S and 52° S, a continuous ice sheet growth is reached by nearly all ensemble members with an overall good match for both eastern and western margins of PATICE. Finally, in the third zone between 38° S and ~~42~~44° S, PIS growth is not uniformly captured by the ensemble members, with most of them failing to build a consistent ice cover.

Among the PMIP climate model products tested in this study, ~~INM-CM4-8~~ AWI-ESM-1-1-LR and MPI-ESM1-2-LR models (both from PMIP4) produce the most consistent ice sheet extents relative to the PATICE reconstruction ~~.~~ (Fig. 1). The near-surface air temperature and precipitation patterns derived from these two climate models enable the modelled ice sheet to reach as far north as 39° S and 40° S, respectively, and occupy total areas of ~~519,552 and 423,360~~ 467,776 and 564,096 km^2. This is in broad agreement with the earlier estimations by Davies et al. (2020). Total ice volumes produced by these two simulations are ~~532.4103 and 417.0103~~ ,347,020 and 471,859 km^3, corresponding to SLEs of ~~1.47 and 1.15~~ 1.04 and 1.37 m (Fig. ~~??k,l~~4), respectively. In the following, we zoom in on the drivers of the dissimilar model performances across these three distinct zones.

3.2 ~~Excessive Patagonian ice cover in south-eastern Patagonia~~

3.1.1 Excessive Patagonian ice cover in south-eastern Patagonia

Our model experiments show that across ~~southernmost~~ southern Patagonia (52° S to 56° S), most ensemble members exhibit an unrealistic build-up of ice, with a much larger eastern ice extent than inferred from the geological evidence (Fig. ~~??~~4). In some cases (e.g., ensemble members driven by CCSM4, GISS-E2-R, MIROC-ESM, ~~and MRI-CGCM3~~Trace21ka, CESM2-FV2 and CESM2-WACCM-FV2), this excessive ice cover reaches what is at present the Atlantic coast. ~~The LGM/PI annual mean precipitation anomalies vary significantly among models for this area (Figs. ??a and ??f). While some of the climate models show a precipitation increase by up to 50 % at 52° S when compared to the PI climate, other models suggest much drier conditions in the same area (up to -50 %). Regarding near-surface air temperatures, we observe a uniform range of LGM-PI anomalies, with most climate models suggesting averaged values within the range of -8 to -6 (Figs. ??b,f). In this region, CCSM4 and MRI-CGCM3 exhibit the coldest conditions relative to the PI, while displaying precipitation increases of up to 20 %. This combination of climate conditions leads to a strong ice sheet advance towards and beyond the eastern~~ We associate the excessive growth towards the eastern side with relatively cold conditions on the leeward side of the Andes, accompanied by relatively larger precipitation amounts when compared with the multi-model mean. These climate conditions reduce the ablation, allowing the ice sheet to advance beyond the margins of the PATICE reconstruction.

Ensemble members that reproduce ~~a reasonable extension require LGM-PI~~ an extension comparable with the geological reconstruction of PATICE showcase positive LGM temperature anomalies of around ~~-6~~ 2 °C, combined with ~~a dry LGM/PI precipitation anomaly of about -20 %~~ drier conditions when compared with multi-model mean (Fig. ~~??f,~~ 2, 3, see climate models ~~AWI-ESM, MIROC-ES2L, MPI-ESM~~AWI-ESM-1-1-LR, MPI-ESM1-2-LR, CNRM-CM5).

3.2 ~~Low sensitivity of ice sheet extents to climate uncertainty in mid-Patagonia~~

~~Between 42~~

3.1.1 Ice sheet extents and climate uncertainty in mid-Patagonia

Between 44° S and 52° S, the model ensemble ~~show~~ shows a relatively low sensitivity to the climatic uncertainty provided by the PMIP models used in this study. ~~Between 44° S and 52° S, a~~ A continuous ice sheet build-up is reached by most ensemble members, with an overall good match along both the eastern and western margins constrained by the PATICE data. Although temperature and precipitation ~~anomalies~~ within the margins of the geologically reconstructed PIS at these latitudes show a large ~~dispersion, ranging from -9 to -3 (LGM-PI) and from -30 to 25 % (LGM/PI), respectively (Fig. ??e~~spread (Fig. 2, 3), this does not lead to drastic changes in the resulting ice sheet extents. ~~However, differences can be observed when comparing the modelled ice sheet thickness under different climate regimes. Under colder (LGM-PI) and wetter (LGM/PI) conditions, the modelled mean ice thickness of PIS increases. In the opposite case of warmer (LGM-PI) and drier (LGM/PI) conditions, the modelled mean thickness decreases.~~ The eastern expansion of the modelled PIS seems to be linked to the summer temperature

in eastern Patagonia, inhibiting the melting during the summer season, despite the reduced precipitation (Fig. 3).

~~This is in stark contrast with the relative performances of these models north of 44 °S, where climate conditions provided by COSMOS-ASO, IPSL-CM5A-LR and AWI-ESM-1-1-LR are only able to build fragmented ice structures (Figs. ??c,f,j), with the main body of the ice sheet not advancing further north of ~ 44° S. The resulting ice sheet temperatures are linked to a temperature anomaly (LGM-PI) threshold equal or colder than -5 and a precipitation ratio (LGM/PI) of at least 1. These thresholds establish the minimum conditions needed to promote PIS advance north of 44° S (Figs. ??a,b,d,e).~~ The forcing from MIROC-ES2L generates LGM climate conditions that lead to the smallest PIS in the ensemble. Due to relatively high air temperatures, all ice accumulated during a model year is lost during the ablation season, preventing ice sheet growth and thus an extent that matches the PATICE reconstruction.

3.2 ~~Drivers of model failure in northern Patagonia~~

3.1.1 Drivers of the lack of ice in northern Patagonia

The PIS growth towards its northern confines is not uniformly captured by the ensemble. Most of the PMIP climate products tested here do not allow for an ice sheet expansion north of ~~42~~44° S (Fig. ??4), while the geologically constrained northern ice sheet margin is placed at 38° S (Davies et al., 2020). As stated earlier, positions of the former PIS margins derived using the AWI-ESM-1-1-LR, INM-CM4-8, MPI-ESM-P and MPI-ESM1-2-LR products are closer to those inferred from the PATICE data set ~~. Although~~ on its northern margin. However, the forcing from ~~AWI-ESM-1-1-LR enables an ice-covered area close to the reconstructed northern boundary (similar to the resulting ice extents from the MPI-ESM1-2-LR ensemble member), the ice cover produced by this simulation cannot qualify as an ice sheet north of 44° S, but rather as an~~ MPI-ESM-P in this area produces a fragmented ice cover that resembles an isolated ice cap ~~(Fig. ??j). Towards the northernmost part of the geologically constrained PIS extent (north of 40° S), none of the ensemble members is able to reproduce the reconstructed ice cover. However, a few ice bodies resembling ice caps are generated by the simulations driven by GISS–E2-R and MPI-ESM-P (Figs. ??c,h~~disconnected from the main ice sheet (Fig. 4).

~~Between 40° S and 42° S, the~~ The modelled climate from INM-CM4-8 ~~model~~ showcases a pronounced reduction in precipitation rates during the LGM~~relative to the PI, reaching a -40 % drop at~~ , with a decline of up to -50 % around 40° S, leading to significantly drier LGM conditions (Fig. ??a). ~~This contrasts all other climate simulations (from both PMIP3 and PMIP4), in which LGM precipitation rates are either equal to or even larger than (up to 10 %) their corresponding PI values (Figs. ??a~~ 3). Conversely, AWI-ESM-1-1-LR, ~~d)~~MPI-ESM-P and MPI-ESM1-2-LR indicate relatively wetter conditions than INM-CM-8, accompanied by a comparable ice sheet extent. Meanwhile, MRI-CGCM3 depicts the highest precipitation amounts in the zone, however with ice-free conditions. Despite these significantly wetter conditions (25 to 50 % larger precipitation rates than in the INM-CM4-8 model), these ensemble members fail to initiate an ice sheet in this region.

In the same ~~range of latitudes, most PMIP3 and PMIP4 models show LGM-PI~~ latitude range, models with ice extent comparable to the geological reconstruction consistently depict colder LGM summer mean temperatures than the multi-model mean, with temperature anomalies ranging from -3 to -6 °C ~~, while~~ relative to the multi-model mean. INM-CM4-8 ~~infers~~ shows a much

larger temperature anomaly, reaching ~~a value of -11~~ -10 °C around 40° S. However, this anomaly ~~suddenly decreases~~ diminishes towards the northernmost margin of the PIS, preventing ice sheet growth there under precipitation-starved conditions (~~Figs. ??b,d~~Fig. 3). In this part of Patagonia, climate forcings from AWI-ESM-1-1-LR, INM-CM4-8 and MPI-ESM1-2-LR thus stand out as the only PMIP model products providing atmospheric conditions that enable the growth of an ice sheet in agreement with the PATICE data set.

Our results highlight the critical role of ~~regional air~~ the summer mean temperatures in the inception and expansion of the PIS over the northern ~~sectors. On the one hand, drier~~ sector. Drier but colder climate states ~~are able to provide a set of conditions that promote~~ can foster ice sheet advance~~. On the other hand, wetter but warmer climates (i.e., mean annual anomaly of around -7) tend to prevent~~ , while wetter yet warmer climates tend to impede ice accumulation despite relatively high ~~rates of precipitation . These findings underline~~ precipitation rates (Fig. 2, 3). These results underscore the importance of ~~reduced~~ minimizing modelled temperature biases ~~as a prerequisite~~ for robust model-based reconstructions of ~~the~~ Patagonian glacial history.

3.2 Evolution of the PIS through MIS3 and MIS2

The timing of the local maximum in the ice volume and the subsequent deglaciation has been documented at multiple locations in Patagonia and recently compiled in Davies et al. (2020). This data set indicates that the former PIS reached its maximum extent at around 35 ka, preserving relatively stable conditions until 25 ka. Here we use the PMIP4 climate model MPI-ESM1-2-LR as the best fitted model to perm our transient simulations (See sec. 2.3).

~~Our results suggest that in order to enable a PIS build-up north of 40º S that matches the PATICE reconstruction, mean annual temperature anomalies (LGM-PI) of at least -5 and precipitation ratios (LGM/PI) close or above to 1 are required. Although some of the climate models exhibit much wetter conditions during the LGM –with precipitation rates being up to~~ For a better spatial comparison, we show the modelled extension of the PIS at 35, 30~~% higher than during the PI in this region (~~, 25 and 20 ka to enable a direct evaluation against the corresponding time slices from the PATICE reconstruction (See section 2.3, Fig. ??) -, they also produce smaller anomalies in temperatures (-2 to -4 , see Figs. ??a-c).Such climate conditions appear too warm to maintain a positive surface mass balance, thus prohibiting ice sheet inception or advance. In this context, the combination of near-surface air temperatures and precipitation rates from GISS-E2-R seems to define an absolute minimum threshold for the presence of an ice sheet~~ 5).

The cores ODP-1233 and MD07-3128 show a quite similar pattern, with a low glacial index during the beginning of MIS3, and then reaching ~ 1.3 during 45 and 50 ka, respectively. Subsequently, both records demonstrate local fluctuations ranging between 0.6 to 1.3. The glacial index derived from MD07-3128 exhibits a slightly negative trend from 50 to 25 ka before experiencing an increase, reaching peak values at 20 ka. Despite their geographical separation, both cores depict transitions from glacial to interglacial conditions almost concurrently, indicating a robust regional capture of PIS dynamics (Fig. 5). Both simulations lack ice in northern Patagonia ~~.~~ (at the northern tip) and are generally smaller than the geological reconstruction of PATICE at 35, 30 and 25 ka. Nevertheless, during the LGM, the ice volume range between the estimates by Wolff et al. (2023) and PATICE (Davies et al., 2020).

The off-shore record GeoB3327-5 shows the highest glacial index prior LGM, reaching maximum values of 3.3 at $\sim$ 45 ka, declining until it reaches values below 1 at around 18 ka (Fig. 5). Our transient simulations forced by this offshore core record showcase similar ice volumes for the time slices at 35, 30, and 25 ka to those proposed by PATICE (Fig. 5). However, the region covered by the ice sheet does not match completely the geological reconstruction, overestimating the extent in northeast Patagonia in several time slices (Fig. 6).

~~Modelled thickness of the PIS and ice base velocity streamlines for the LGM. The green line shows the reconstructed glacier extent from the empirical evidence at 20 (Davies et al., 2020). The present-day coastline is shown for reference.~~ The off-shore record PS75/034-2 shows a glacial index in the range 0.3–0.6 between 70 and 40 ka, with a steady increase between 38 and 30 ka that brings the glacial index to a value above 1, reaching a maximum at $\sim$ 18 ka, and finally followed by a rapid drop (Fig. 5). These conditions lead to a small ice sheet at 35 ka, which is still growing by 30 ka, with a more stable condition during 25 and 20 ka when it reached a closer extent to the PATICE reconstruction (Fig. 6) with an ice volume of 400.000 km^3 which is between the two most recent estimations (Fig. 5).

Our results using Antarctic records suggest a maximum ice volume of PIS closer to the global LGM, characterized by continuous ice mass growth between the MIS3 and the MIS2 (Fig. 5). On the one hand, the Siple Dome ice core shows glacial index values below 0.5 during most of MIS3, with an increase that begins at 30 ka, reaching a value of 1 around 20 ka, and a maximum even later closer to 15 ka. These conditions lead to a small PIS during MIS3 with an ice volume of 100.000 km^3 until 25 ka, when the ice sheet starts to increase, reaching 400.000 km^3 at 20 ka. However, the maximum extension and volume are reached even later at 15 ka. On the other hand, EDC shows a glacial index that starts to increase during the beginning of MIS3, reaching a maximum at 25 ka, with values that keep closer to 1 until 18 ka, marking a change in its trend with an abrupt decrease. In terms of ice volume, our simulation achieves stable conditions between 25 to 18 ka with 380.000 km^3. While the extension reproduced at 20 ka is reasonable, both cores exhibit a completely different glacial history when compared with the geochronological dataset of PIS (Fig 6).

4 Discussion

~~In this section, we first examine the correspondence between the PMIP paleoclimate model experiments and available constraints from empirical paleoglacial and paleoclimate evidence across Patagonia. In this context, we focus on quantifying whether model-based climate reconstructions are consistent with the reconstructed Patagonian ice sheet geometry over different sectors of formerly glaciated Patagonia. Then, we identify potential impacts of the prescribed topographic forcing and horizontal climate model resolution on the modelled climate conditions. Finally, we discuss our findings in the context of asynchronous glaciation histories between the PIS and paleo ice sheets in the northern hemisphere, considering the limitations arising from the assumption of an ice sheet equilibrium with the climate of the Last Glacial Maximum (LGM).~~

4.1 ~~Performance of PMIP models in Patagonia: Phase 3 versus Phase 4~~

Here, we take a closer look at the PMIP models and their regional behaviour across Patagonia, zooming in on the differences between the reconstructed monthly mean temperatures and precipitation rates. Some of the largest differences between model performance in the two phases of PMIP are related to the fact that PMIP3 anomalies show stronger cooling during the austral winter and weaker cooling during summer which tend to accentuate the amplitudes of the annual temperature cycle (Fig. **??**).This is in contrast with the outputs of individual PMIP4 experiments, where MPI-ESM1-2-LR has similar characteristics to PMIP3 models, while MIROC-ES2L produces stronger negative temperature anomalies during the summer-early autumn period (January-April). In contrast, precipitation ratios show a high dispersion across seasons and models. In general, most models exhibit a general decrease in precipitation, particularly in the mean annual rates, even though some models infer an increase in winter precipitation. The exception is CNRM-CM5, which shows a general, albeit relatively small increase in both mean annual and winter precipitation rates. When looking at the sub-regional (sector-scale)performance of PMIP climate, it becomes clear that most of them

4.1 Performance of PMIP models in Patagonia

At the sub-regional scale, most PMIP models fail to reproduce the reconstructed extents climate conditions required to simulate the extent of the northernmost sectors sector of the PIS during the LGM (38-42as suggested by reconstructions. As we show in Sect. 3, the models that produce the most realistic extents of the PIS between 38-44° S). To investigate the origin of this behaviour, we have calculated average temperature and precipitation anomalies within the former PIS outlines between 38° S and 42° S (Fig. **??**). Latitudinal annual means of a) the LGM/PI precipitation ratio and b) temperature anomaly within the geologically reconstructed area of the former PIS (LGM-PI) (Davies et al., 2020). Shaded areas show the envelopes between the INM-CM4-8 and MPI-ESM1-2-LR. Annual mean precipitation ratio and temperature anomalies, including mean annual standard deviation through the year between c) 38° S and 39° S, d) 40° S and 42° S, e) 46° S and 52° S and f) 52° S and 56° S. LGM-PI temperature anomalies (upper panel) and precipitation anomalies (bottom panel) for the monthly outputs of CMIP5-PMIP3 and CMIP6-PMIP4 averaged over the study zone. LGM-PI temperature anomalies (upper panel) and precipitation anomalies (bottom panel) for the monthly output of CMIP5-PMIP3 and CMIP6-PMIP4 calculated of the northernmost sector of the former PIS. Calculations are made over the grid points that match the reconstructed PIS extents by Davies et al. (2020) within the 38-42° S study zone. Large differences can be observed in the climate model reconstructions when looking at their particularities in this regionare those that exhibit the coldest LGM temperature during the melting season. The models AWI-ESM-1-1-LR, INM-CM4-8, and MPI-ESM1-2-LR suggest generate larger negative temperature anomalies during the melting season when compared against the multi-model mean. In particular, INM-CM4-8 stands out by producing very cold conditions during the LGM nearly throughout the entire year, with a higher amplitude during January and February (austral summer) (Fig. 2, 7). Its drop in near-surface temperatures of around 12 during the melting season is an outlier, showing a difference of at least 4 relative to other PMIP4 models. Lower temperatures inferred from INM-CM4-8 act as a driving mechanism for the realistic an ice sheet growth between 38-4238-44° S. The temperature anomaly suggested by INM-CM4-8 is less intense during winter months, being closer to the range of inferred from the other models .MIROC-ES2L produces the smallest LGM-PI temperature anomaly among all PMIP4 models, with an annual mean of around 4 . While MPI-ESM1-2-LR

Although the forcing fields from other models such as MPI-ESM-P and ~~AWI-ESM-1-1-LR reproduce relatively similar annual cycles, MPI-ESM1-2-LR provides 0.5 colder temperatures in the annual mean~~ CNRM-CM5 manage to build up ice towards the north of the domain — again due to relatively colder conditions —, the resulting glaciated areas resemble isolated ice caps rather than an extension of the PIS (Fig. ~~??. In contrast, PMIP3 models show two types of patterns - one similar to PMIP4 models and another with pronounced cooling. The first group of experiments (GISS-E2-R, IPSL-CM5A-LR, and MPI-ESM-P) results in smaller temperature anomalies between the LGM and PI summers, while other models show a greater cooling during the winter, with some having larger cooling amplitudes (e.g. CCSM4 and MRI-CGCM3)~~2). Despite colder conditions, the simulations driven by these models are still unable to reconstruct the formerly PIS-covered territories north of 39° S.

~~Regarding the reconstructed precipitation rates, PMIP3 and PMIP4 exhibit significant differences. It is apparent that no common mean-annual precipitation patterns can be revealed~~ Similarly, the eastern expansion is consistently associated with a negative temperature anomaly when compared with a multi-model summer mean (Fig. ~~??). Most models predict months with positive or negative anomalies throughout the year, except for INM-CM4-8, MIROC-ES2L, and MRI-CGCM3, which consistently generate lower-than-PI precipitation ratios for all months that are close to the lowest end of the total range. All other models tested here exhibit an overall increase in the annual mean precipitation rates in this region, with CNRM-CM5 and FGOALS-g2 generating the wettest conditions among all models~~2). As shown by the simulation driven by CNRM-CM5, relatively warmer conditions in the southern-east sector of Patagonia are required to restrict the extension of the PIS within its geologically reconstructed margins (Fig. 2), coincidentally being the model that shows the best fit in this zone. Compared to air temperatures, precipitation does not seem to play a dominant role when analysing the causes for PIS over-expansion in this region.

~~As we show in Sect. 3, the models that produce the most realistic modelled extents of the PIS between 38-42° S are those that exhibit the strongest negative LGM-PI temperature anomalies (-8 to -12) during the melting season. These models are INM-CM4-8 and MPI-ESM1-2-LR, although the northward ice sheet advance resulting from the latter only reaches 40° S (Figs. ??k,l), leaving the formerly PIS-covered territories between 38° S and 40° S ice-free. This is because the (LGM-PI) temperature anomaly derived from MPI-ESM1-2-LR is at least 4 lower than in INM-CM4-8, which displays a drastic drop in the temperature anomaly (between -12 and -10) towards the north of Patagonia~~ The forcing from MIROC-ES2L produces the smallest modelled ice sheet geometry among all the climate models considered in this study (Fig. 4). Its summer mean temperature is the warmest, only comparable with MRI-CGCM3. Differences between the two resulting ice sheets can be explained by dissimilar winter temperatures, which in the case of MIROC-ES2L restrict accumulation during the cold season, preventing a realistic build-up (Fig. ~~??b~~2, 3).

~~Paleo-vegetation records at 41° S infer 6~~ Previously, Yan et al. (2022) analysed 21 PMIP model outputs of phases 2, 3, and 4, to ~~7 colder mean annual temperatures during the LGM than at present (Moreno et al., 1999). When these reconstructions are combined with the glacial geology and palynology data collected within 40-42° S, we arrive at a range of 6 to 8 colder mean summer temperatures and 6 to 7 colder mean annual temperatures at LGM (Denton et al., 1999). On the one hand, these data suggest that the cooling of ~ 12 observed in INM-CM4-8 during summer months is relatively extreme compared to~~ infer the climate conditions for ice sheet growth. Despite efforts to fuse PMIP models with present-day data, models

struggled to reproduce ice sheet extent accurately, showing lack of ice in the north and overexpansion in the south east. Cuzzone et al. (2023) investigated PMIP4 models in a narrower domain, finding similar issues despite higher resolution. Both studies fused paleoclimate anomalies with present-day data, inducing artefacts in heterogeneous climates. However, the ~~range observed in existing proxy records. On the other hand, the AWI-ESM-1-1-LR and MPI-ESM1-2-LR models arrive at summer anomalies that are consistent with the constrained range. However, annual mean temperature anomalies in these two models are close to -5 , which is 1 below the lower limit of the suggested range (Fig. **??**d). By comparison, INM-CM4-8 infers a value of around -8 , which overestimates the reconstructed cooling by 1 . Nevertheless, among all models tested in this study, AWI-ESM-1-1-LR, INM-CM4-8 and MPI-ESM1-2-LR produce temperature anomalies that are closest to the available paleoclimatic records in northern Patagonia .~~ lack of grounded-based validation data in southern mid-latitudes limits the skill of reanalysis data in Patagonia (Masiokas et al., 2020; Sauter, 2020). ~~It is difficult to infer what factors are responsible for this regional scattering between different phases of PMIP , mainly due to the number of changes~~ Several factors might be responsible for the large regional scattering among model results from different PMIP phases, including significant updates between model versions, ~~e.g.,~~ the treatment of vegetation, atmospheric dust loading, and prescribed ice thickness and topography (Kageyama et al., 2017). The latter ~~,~~ in particular, ~~raises questions about the importance~~ exposes a circularity problem in which model reconstructions of the PIS ~~for shaping regional climate regimes during the LGM and its impact on modelled atmospheric states~~are driven by climate conditions that include a poorly resolved (or inexistent) ice sheet (Section 4.2). This highlights a need for studies providing a benchmark for the effects of topographic and albedo ~~feedbacks (among others)~~ feedback between the PIS and the regional climate dynamics. ~~Previously, Yan et al. (2022) modelled the PIS during the LGM using climate forcing products from phases 2, 3 and 4 of the PMIP project. To achieve a good fit with geological evidence, the PDD factors in the surface mass balance (SMB) model were reduced to promote ice sheet growth. However, the applied PDD factors in this earlier study are not supported by existing studies of present-day ice sheets (Peano et al., 2017; Seroussi et al., 2020) or ice fields in Patagonia (Möller and Schneider, 2008; Bown et al., 2019), indicating that this evaluation may be biased due to the choice of model parameters. The best fit with the reconstructed ice sheet configuration in Yan et al. (2022) was achieved using MPI-ESM1-2-LR output, while the forcing using INM-CM4-8 resulted in a much larger PIS. Our findings indicate that using a set of model parameters that is consistent with the current knowledge leads to an underestimation of ice sheet extent in the north of Patagonia, as observed in the experiment driven by MPI-ESM1-2-LR, while the climate conditions from INM-CM4-8 still allow for a more extensive ice coverage, albeit with a less over-expansion.~~

4.2 Impacts of the PMIP topography and resolution

~~In Sect. 3 we show that, under the chosen parameters (Table 1), none of the experiments carried out in this study were able to build an ice sheet in agreement with the reconstructed PIS geometry (Fig. **??**). It has become clear that all PMIP models struggle to reproduce air temperatures that are consistent with both local proxy records and geological reconstructions of the former ice sheet extents in northern Patagonia (Figs. **??**b,c,d). Due to the fact that the northern sector of the PIS is a relatively narrow ice mass that resided in an area of exceptionally steep topography (Fig. **??**), here we analyse to which extent this important factor for the ice sheet growth is reproduced by the PMIP climate models, and whether the typical lack of resolution~~

~~in global models may be a possible origin of such a struggle. Furthermore, the ice sheet~~ The ice sheet forcing itself is an important component of paleo experiments, introducing regional-scale climate feedback through additional topographic barriers and the albedo effect (Löfverström et al., 2014; Beghin et al., 2015; Liakka et al., 2016). ~~In this context, it is important to note that participants of PMIP~~ PMIP participants used different ice sheet ~~forcings in different project phases: the~~ reconstructions: PMIP3 ice sheet reconstruction (Abe-Ouchi et al., 2015), ~~the~~ ICE-6G_C (Peltier et al., 2015), and GLAC-1D (Tarasov et al., 2012). ~~All these reconstructions are sufficiently different from each other, leading to deviations~~ The difference between these topographic forcings led to a large spread in climate model results (Abe-Ouchi et al., 2015).~~In addition, dissimilar horizontal resolutions within climate models may induce further differences in modelled climate regimes on a regional scale (Table 2). Here we focus on the analysis of PMIP4 topographic forcings and the differences between them. We expect that our observations and conclusions based on the analysis of PMIP4 models will be broadly applicable to other phases of PMIP, except that most of the earlier PMIP phases did not include an ice sheet forcing in Patagonia (Kageyama et al., 2017).~~

~~Prescribed topography (upper panel) and ice thickness (bottom panel) by the PMIP4 models considered in this study. Etopo-1 (Amante and Eakins, 2009) and the ICE-6G_C reconstruction (Peltier et al., 2015) included as of the ice sheet forcings in PMIP4. The Cyan line shows the PIS extension for the 20 ka (Davies et al., 2020). Present-day ocean-continent limits are shown for interpretation.~~ PMIP4 models used in ~~this study apply dissimilar topographic forcings, mainly due to modifications to meet~~ our study vary in topographic forcing due to the spatial resolution imposed in each of them. ~~In Patagonia, all models include simplified topographic features that do not exceed 1500 m in altitude (Fig. ??). Furthermore, these simplifications shift~~ All models simplified the topography, shifting the position of the Andes and ~~flatten~~ flattening the observed topography, which ~~exceed~~ exceeds 3000 m above sea level in the north (Fig. **??**) ~~. Regardless of its good ice-covered area agreement against PATICE, the topographic forcing of INM-CM4-8 (which has the finest latitudinal resolution among PMIP4 climate models) has undergone visible substantial modifications (Fig. ??). INM-CM4-8 does feature a higher topography in the northern part of the model domain, where it might accentuate colder and drier LGM climate conditions. This suggests that a much higher spatial resolution is needed to capture the atmospheric dynamics and climate gradients over the complex terrain and extreme environment of the Andes when using general circulation models (Bozkurt et al., 2019).~~ 8) but only reaches a maximum of 1500 m when applied. To compare the ~~ice sheet thickness and ice-covered area of each PMIP4 ensemble member~~native PMIP4 ice sheet thicknesses and coverage, we compute the difference between the LGM and the PI topographies~~assuming that the sea level during LGM~~ , assuming LGM sea level was 120 m lower~~than present. The ice mask provided by each ensemble member is then used to delimit the ice sheet geometry. If we focus on the PMIP 4 models alone, we can observe that ice sheet~~ . Ice sheet geometries prescribed in the AWI-ESM-1-1-LR, INM-CM4-8 and ~~MPI-ESM1-2_LR climate experiments are broadly consistent with the north-to-south extents of the former PIS~~ MPI-ESM1-2-LR climate experiments broadly align with the former PIS extent derived from the geological evidence (Davies et al., 2020). ~~This does not imply, however, that the prescribed PIS in any of these climate models is necessarily accurate (Fig. ??). This is particularly evident in the prescribed ice sheet within~~ However, this alignment does not guarantee an accurate PIS representation. MIROC-ES2L ~~, which is~~ and CESM-WACCM-FV2, the coarsest climate ~~model among the four PMIP4 models analysed that fails~~ models analyzed, fail to reproduce LGM climate conditions that enable our ice sheet model to build an ice sheet extension consistent with PIS north

of 44° S (Fig. ??). Within the geologically constrained ice-covered area, our comparison of monthly anomalies in near-surface mean air temperatures reveals large discrepancies between the four PMIP4 models north of 46° S (Fig. ??b,c,d). 4). For example, INM-CM4-8 infers a more negative anomaly compared to the three other models, peaking at a mean annual value of nearly -12 at around 40° S. At this latitude INM-CM4-8 prescribes an ice thickness of around 300 (Figs. ?? and ??), whereas MIROC-ES2L does not include any ice sheet forcing in this area. As a consequence, the latter generates much higher mean annual temperatures, with an LGM-PI anomaly amounting to only -3 . This implies that in this geographical sector, the two models placed at the extreme ends of the spectrum of possible regional thermal climate regimes are separated by 9 . Although AWI-ESM-1-1-LR and MPI-ESM1-2-LR have relatively similar ice sheet boundary conditions at these latitudes when compared to INM-CM4-8, they both arrive at smaller temperature anomalies north of 42m north of 46° S, leading to a limited expansion of the PIS and ice sheet fragmentation (Fig. ??).whereas MIROC-ES2L includes no ice sheet at all.

(a) Hypsometric curves of prescribed ice forcings in the PMIP4 models against the reference ICE-6G_C geometry. Mean ice thickness for each model is shown in vertical lines. Mean topography between (b) 38º S to 42º S, (c) 42º S to 52º S and (d) 52º S to 56º S. The PMIP4 topography of each member is shown in dashed and continuous lines for its PI and LGM time periods, respectively. Our simulations suggest that most PIS sectors had an ice thickness between 1000 and 1500 , with a maximum close to 2000 . Such thick ice cover should have greatly impacted regional climate conditions during the LGM. In one of the most problematic regions, located between 38° S to 42° S, PMIP experiments prescribe an ice sheet that peaks at a thickness of around 300 , while our experiments suggest a likely range of thickness values between 200 and 700 over this area.However, it appears difficult to constrain the regional ice sheet thickness and extent using geological reconstructions that are very fragmented and lack direct constraints on the former ice surface elevations (Boex et al., 2013; Troch et al., 2022) .Towards the south-eastern sectors of the PIS, our results showcase findings reveal a consistent overestimation of modelled ice sheet extents relative to the geological evidence. We partially attribute this excessive ice sheet growth to the mismatch between to the discrepancies between reconstructed PIS coverage and the prescribed topography in the climate models: ice climate models. Ice sheets invade formerly ice-free territories, potentially promoting inducing extra cooling and leading to reduced ablation . The rather poor performance of climate models along leeward slopes of the Andes can be therefore partly attributed to unrealistic ice sheet forcings that lost their outlines and spatial details during spatial upscaling. Other potential contributing factors to this unrealistic ice sheet growth in the south-east include erroneous albedo forcings and a lack of orographic effects due to unresolved precipitation barriers (Fig. ??b,c,d). Erroneous reduced ablation through a stronger albedo forcing. Inaccurate representation of the orographic effect on precipitation is very likely a contributor to the likely exacerbates mismatches between the modelled and reconstructed ice sheetsin this area due to very strong flattening of the topographic forcing (including mountain ranges and prescribed ice sheets), and thus its inability to impose the , as topographic forcing is flattened (Fig. 8), hindering the imposition of the rain-shadow effect under these horizontal coarse resolutions (Lofverstrom and Liakka, 2018; Bozkurt et al., 2019; Almazroui et al., 2021). The lack of this effect leads to This deficiency results in reduced precipitation on the windward side but much higher precipitation on the leeward side of the Andes, promoting the growth and eventually overflow of the PIS fostering PIS expansion beyond its geologically constrained eastern margin.

Studies of former ice masses in the Northern Hemisphere have been used to Norther Hemisphere ice masses demonstrate that

under the same orbital and greenhouse forcings, ~~discrepancies between~~ differences in the ice sheet boundary conditions ~~in otherwise identical experiments lead to robust, large-scale~~ yield significant impacts on the atmospheric circulation and temperature (Ullman et al., 2014; Löfverström et al., 2014; Bakker et al., 2020; Izumi et al., 2023). ~~The PMIP models are able to reproduce the general~~ PMIP models generally capture temperature and precipitation conditions over South America during the LGM (Berman et al., 2016)~~. However, due to their resolution they are unable to reproduce~~ , yet lack the resolution needed for detailed regional climate responses ~~with a necessary detail (Bozkurt et al., 2019). As we have shown, their resolution is generally too coarse to drive modelling studies of the~~ (Bozkurt et al., 2019). Thus, coarse resolution impedes modelling of Patagonia's narrow ice sheet~~in Patagonia since. We strongly suggest that a significantly higher~~ . Higher climate model resolution is ~~needed to study~~ crucial for studing the influence of ~~the Andean topography features on the~~ Andean topography on past regional climate dynamics~~and capture~~ , which requires capturing the longitudinal gradient ~~between the colder and wetter windward side of the Andean mountain range and~~ from the windward to the leeward side.

4.3 Glacial history of southern South America

A recent study has proposed the earlier LGM in Patagonia (Davies et al., 2020) and its consequent earlier deglaciation when compared against the Northern Hemisphere ice mass or Antarctica (Hughes et al., 2016; Batchelor et al., 2019; Gowan et al., 2021) . However, the ~~less cold and drier leeward side. Based on this analysis, we suggest that all PMIP models currently oversimplify the terrain in our target area, distorting the land topography through smoothing, flattening and by prescribing too thin and incorrectly distributed ice cover~~timing of the deglaciation along the PIS is not uniform (Darvill et al., 2015; Peltier et al., 2021; Lira et al., 2 . In the northern part, the geochronological reconstruction proposed a relatively stable margin, with several readvances, between the local and the global LGM (Davies et al., 2020; Leger et al., 2021), with a ~~maximum ice sheet thickness reaching between 700 and 800 (Fig.~~**~~??~~**~~a) as opposed to the expected thickness of up to 2000 (Fig.~~ **~~??~~**~~).~~rapid deglaciation that started at around 20 ka (Moreno et al., 2015; Davies et al., 2020). Conversely, in the southern counterpart, the deglaciation signal is more pronounced before the global LGM, suggesting an earlier local LGM occurring between 30 and 45 ka (Kaplan et al., 2007; Darvill et al., 20 .

~~To summarize, climate models show poor performance both in the south-eastern sector of the former PIS and at its northern tip.~~ As shown in our transient simulations in Sect 3, the glacial index signal based on Antarctic ice cores drives a progressive growth of the modelled PIS through the MIS3 to the MIS2, reaching the maximum extension of the PIS towards the global LGM. In contrast, local off-shore records seem to capture a signal that drives a PIS evolution in agreement with the geochronological reconstruction (Davies et al., 2020). On the one hand, ~~the south-eastern sector reveals an excessive ice sheet growth amounting to up to 400 thick undocumented ice masses in formerly ice-free regions~~ODP-1233, located near the coast in northern Patagonia, reproduces relatively stable climate conditions between 35 and 20 ka. On the other hand, ~~the northern sector of the PIS is lacking ice , partly due to thinner or non-existent ice sheet boundary conditions in PMIP4 climate experiments and too warm climate regimes inferred from most PMIP experiments.~~MD07-3128 exhibits a negative trend during the same period, in correspondence with the reconstructed PIS behaviour south of 52ºS.

The offshore record GeoB3327-5 suggests a climate condition that enables a more extensive ice sheet towards the MIS3. However, it should be taken into account the coarse sampling resolution and the consequent not well-resolved history proposed by them. The extreme glacial index factor induces a large drop in the summer mean temperatures during LGM. The precipitation shows a pronounced decrease in eastern Patagonia, even to zero in some places. This combination does not allow the ice sheet to over expand towards the east.

The southernmost off-shore records analyzed in this study, PS75/034-2, shows a similar behaviour to the Antarctic ice core records. We hypothesize that this core captures a transitional signal between the climatic behaviour of southern mid-latitudes and the Antarctic cores.

4.4 Potential implications of dissimilar LGM timings in the Southern and Northern Hemispheres

~~Here we discuss the limitations of our study design and propose possible ways of overcoming these in future work.~~ The first challenge in this study is related to the assumption of climate and ice sheet equilibrium states during the global LGM. It is~~however~~ , however, an open question whether it is fair to generate PIS model reconstructions assuming that the ice sheet was in a steady-state under global LGM climate conditions ~~, and~~and, if not, how to treat the lack of reliable climate forcing for the earlier periods of the last glacial cycle. The second challenge is related to the interpretation of major planetary drivers that enabled an asynchronous glacial response of the two hemispheres to changes in the orbital and greenhouse gas forcings (Doughty et al., 2015).

The ~~geologically-constrained~~ geologically constrained gap between local LGM timings in Patagonia and different parts of the Northern Hemisphere raises an important question about the drivers ~~of these differences in timing~~behind this asynchronicity. These drivers potentially involve climatic feedback mechanisms, hemispheric climate sensitivities to orbital and greenhouse gas forcings and ~~interactions~~ teleconnections between the two hemispheres (Darvill et al., 2016). The current evidence suggests that the local glacial peak in the southern Andes and Patagonia happened at about 35 ka (Zech et al., 2011; Davies et al., 2020), which is much earlier than the local LGM inferred for most of the paleo ice sheets in the Northern Hemisphere. Aside from the Barents-Kara Sea Ice Sheet and smaller glaciations in Asia, ice masses of the last glacial cycle attained their maximum extents and were driven towards maximum ice volumes during the ~~Marine Isotope Stage~~ MIS 2, at about 24-18 ka, (Hughes et al., 2016; Patton et al., 2016; Gowan et al., 2021) by a strong cooling between 30 and 20 ka. According to the current state of knowledge, these massive ice sheets only began disintegrating at around 18 ka (Patton et al., 2017; Stokes, 2017; Gowan et al., 2021). The situation is ~~however~~ different for the Southern Hemisphere. Due to a lack of large-scale paleo ice sheets and scarce information about past fluctuations of the Antarctic Ice Sheet, it is necessary to look at the existing evidence for the advance and retreat history of smaller ice bodies ~~in order~~ to contextualise the situation in the Southern Hemisphere during the last glacial cycle. For example, records coming from an icefield located in the Southern Alps in New Zealand indicate that this ice mass reached its maximum extent at around 28 ~~ka~~ ka (Rother et al., 2014). According to recent studies, its growth towards 28 ~~ka~~ ka was influenced by a slight decrease in temperatures in the preceding two millennia (Darvill et al., 2016). The reconstructed air temperature cooling at this location is estimated ~~as 6 to~~ to be between 6 and 6.5 °C below present, accompanied by a precipitation reduction of up to ~~-25~~ 25 % (Golledge et al., 2012b). During the period between 26 ~~to~~ and

20 ka, this icefield is thought to have undergone a slow and continuous retreat, followed by a standstill at around 19 ka. This coincides with the time when most of the Northern Hemisphere ice sheets began retreating from their maximum positions due to slowly increasing solar radiation and activation of positive climate feedback mechanisms. Arguably, the Antarctic Ice Sheet seems to have been stable until about 18 ka, after which it experienced an increase in air temperatures synchronised with the increase in CO_2 concentrations (Parrenin et al., 2013; Brook and Buizert, 2018). This triggered the retreat of ice margins in Antarctica, New Zealand, and South America, where the PIS experienced an accelerated retreat starting from 18 ka (Davies et al., 2020). The current evidence of an early local LGM in Antarctica is inconclusive, partly due to an extreme sensitivity of the Antarctic Ice Sheet to the ocean forcing as opposed to the thermal atmospheric forcing playing the largest role in the deglaciation of formerly ice sheet-covered areas (Golledge et al., 2012a). However, pieces of evidence from Patagonia and New Zealand suggest that the Southern Hemisphere might have responded very differently to the global cooling of the last glacial period compared to the Northern Hemisphere (Darvill et al., 2016; Shulmeister et al., 2019).

5 Conclusions

~~We have performed a regional assessment of the PMIP paleoclimate model products (phases 3 and 4) across Patagonia using a~~ Using a combination of ice sheet modelling, ~~paleoglacial reconstructions, and paleoclimate proxy data as a metric for climate model performance. As part of this assessment, we have narrowed down the range of atmospheric conditions needed during the LGM to promote an inception and advance of the PIS in its different sectors, so that they are in agreement with~~ paleoclimate model output, ice and sediment core records, and a recent geomorphological reconstruction, we explore the glacial history of the ~~ice sheet-wide empirical reconstruction PATICE. For this purpose, we have designed~~ former ice sheet in Patagonia, with a focus on the timing of its maximum advance. As an initial assessment, we generate an ensemble of ~~large-scale~~ ice sheet model simulations driven by downscaled~~PMIP climate products to obtain PIS configurations that are in equilibrium with each model-based climate regime. This set of ice sheet model simulations has been used to analyse and interpret the characteristics of contrasting regional climate regimes from ensemble members across different latitudinal sectors of Patagonia. We have observed~~ , constant paleoclimate reconstructions to get a first-order approximation of the extent the PIS can attain under peak global glacial conditions. By evaluating our ensemble against the PATICE reconstruction, we observe that most paleoclimate ~~models provide much warmer atmospheric conditions along the northern segment of the former PIS than those required to initiate the growth of an ice sheet and support its advance towards the geologically reconstructed boundaries. Our analysis indicates that a sector-averaged mean temperature anomaly of at least 5 below the present-day conditionsis needed to generate an ice cover that matches the geological evidence. At the northernmost tip of the PIS,~~ model products provide conditions that prevent the inception of the PIS at its northernmost margins while boosting an overestimated growth in the southeast, in alignment with earlier studies that implement different modelling choices. We perform a latitudinal analysis that reveals a narrow envelope of air temperature and precipitation rate pairs that foster a northern PIS growth in agreement with PATICE, while PMIP models typically showcase much warmer conditions. In contrast, cold air temperatures in the southern PIS and the associated lack of surface ablation prompt an unchallenged advance under too-wet conditions that seem to ignore the Andean

topographic barrier. By investigating the original representation of the region within the PMIP models we find a ~~relatively narrow envelope of PMIP-derived temperature and precipitation anomalies that accommodates a reasonable agreement between the modelled and reconstructed PIS extents. The warmest climate regimes within this envelope correspond to a minimum cooling of approximately -7 accompanied by wetter-than-present conditions with a precipitation increase of around 15 %. The coldest and driest end of the plausible rangeis associated with a more significant cooling of -11 and a reduction in precipitation rates of around 20% to keep the ice sheet from excessive expansion~~topography that is severely flattened along the Andes, which points to the possibility of a diminished rain-shadow effect and subsequent overestimation of precipitation on the leeward side of the mountain range. Our findings highlight the need for a significantly higher climate model resolution to properly capture the complex longitudinal gradients of the Patagonian region.

~~Between 44° S and 52° S, most ensemble members show a continuous build-up~~ To account for the seemingly asynchronous peak glacial advance of the PIS ~~, which is in general agreement with the reconstructed eastern and western ice sheet margins at the LGM. We have constrained an envelope of~~ relative to the Northern Hemisphere ice sheets, we additionally produce an ensemble of transient ice sheet simulations driven by time-evolving climate conditions derived from a variety of ice core and off-shore sediment records. Our results show that the climate forcing based on local sedimentary records is capable of driving a PIS advance that peaks around MIS3. In addition, we find latitudinal differences in the evolution of the PIS between this local peak and the global LGM: southern Patagonia and far-off-shore records exhibit a warming trend during this period, whereas the northern sectors remain relatively stable. In a stark contrast, our experiments reveal that none of these patterns can be reproduced by ensemble members driven by climate conditions based on Antarctic records. This strong connection between the glacial history and regional circulation patterns in Patagonia suggests that the ~~LGM-PI temperature anomalies within this region to a range of -5 to -8 that is accompanied by the range of precipitation rates anomalies between -20 % and 20 % relative to their PI counterparts. In sharp contrast to the results for the northern and southern boundaries, climate models exhibit an overall high degree of agreement within this broad PIS sector.~~ local paleoclimatic signal represents a key component in studies of PIS evolution.

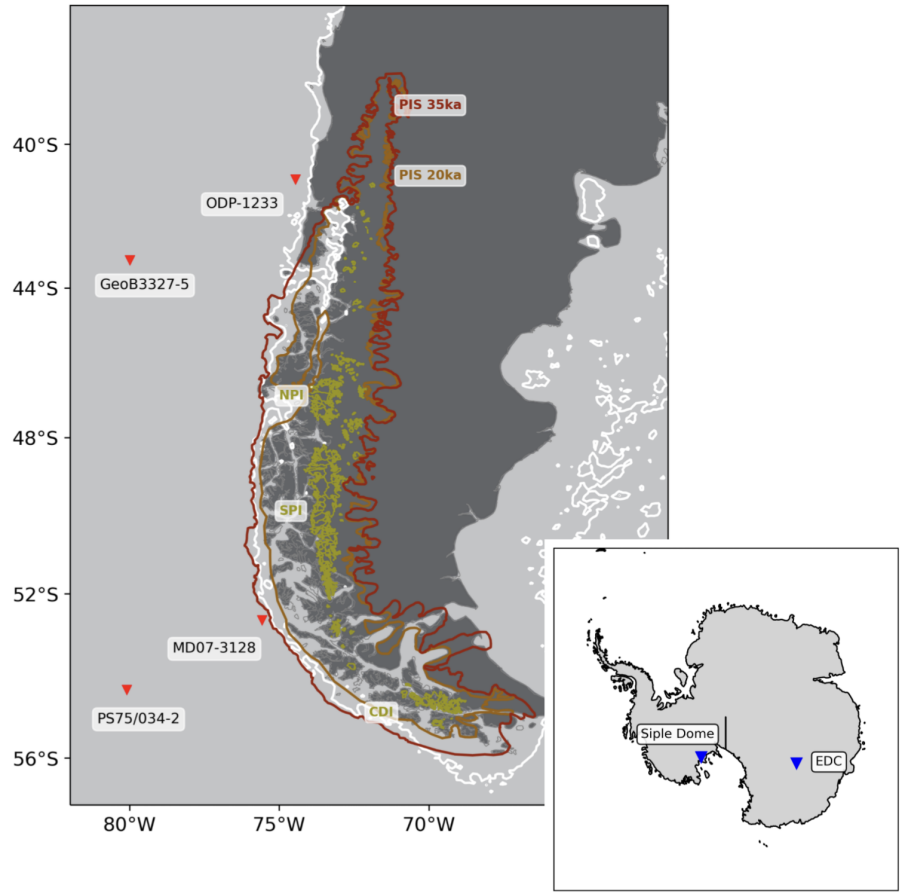

Figure 1. PIS reconstruction of (Davies et al., 2020) for 35 and 20 ka. Present-day ice fields are indicated and correspond to the Northern Patagonian Icefield (NPI), Southern Patagonian Icefield (SPI) and Cordillera Darwin Icefield (CDI). LGM coastal lines marking lower sea level (-120 m) are shown in white.

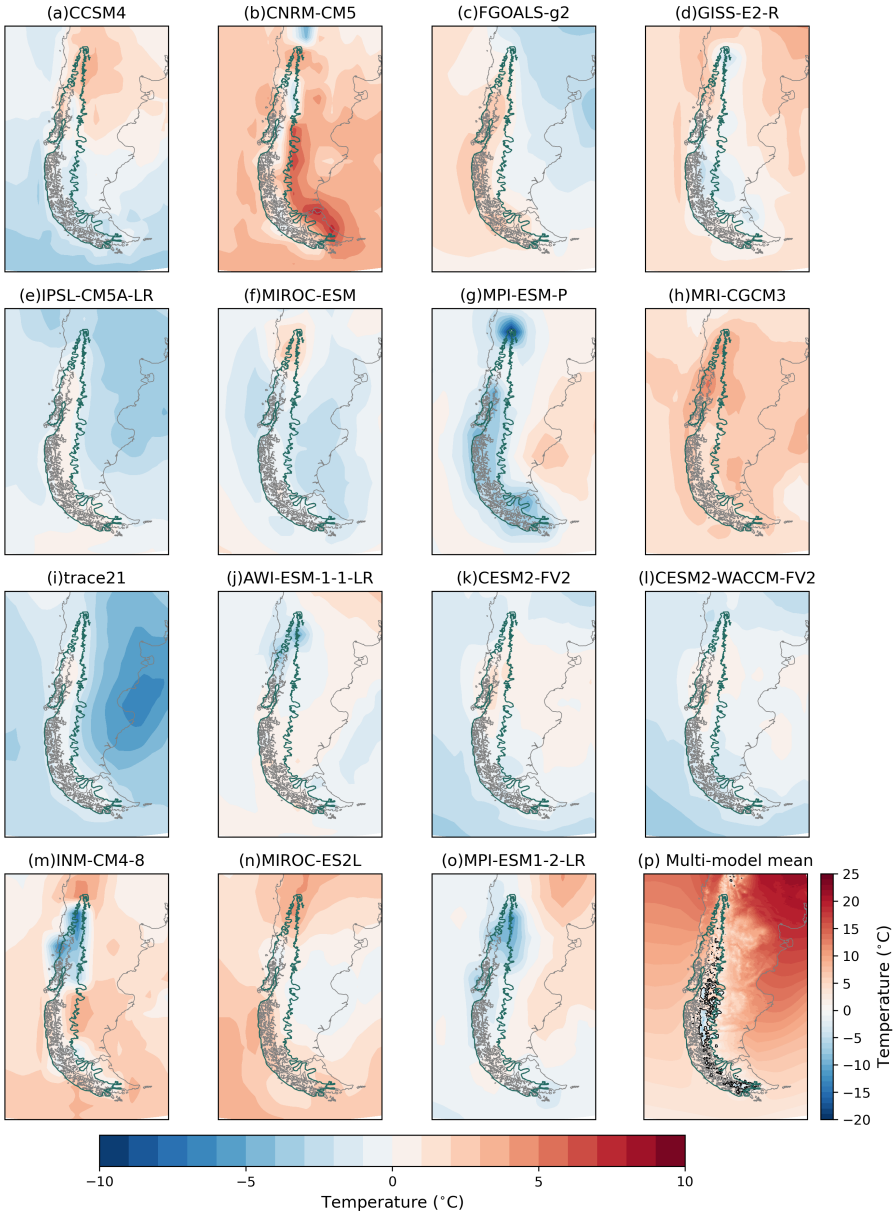

Figure 2. LGM summer mean temperature anomaly with respect to the multi-model summer mean temperature.

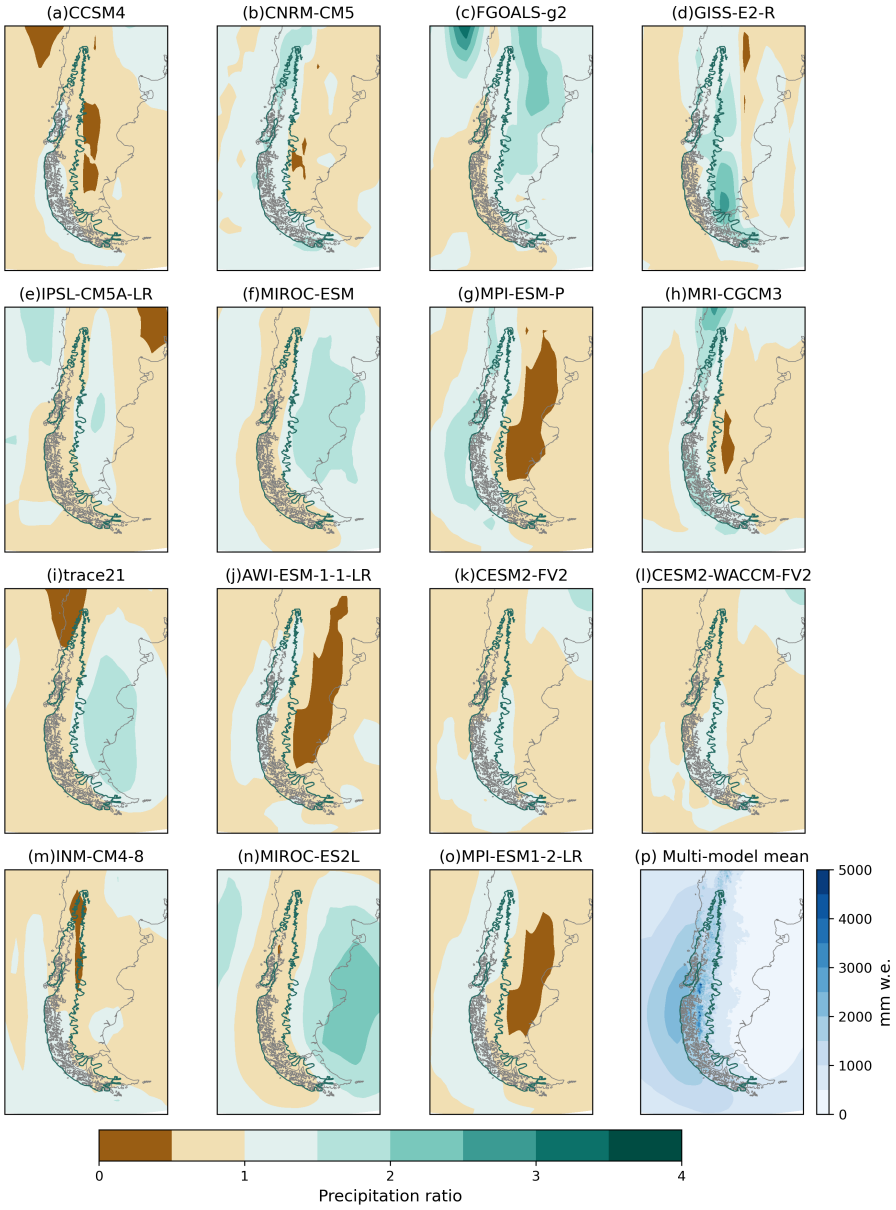

Figure 3. LGM total annual precipitation ratio with respect to the multi-model mean of the total annual precipitation.

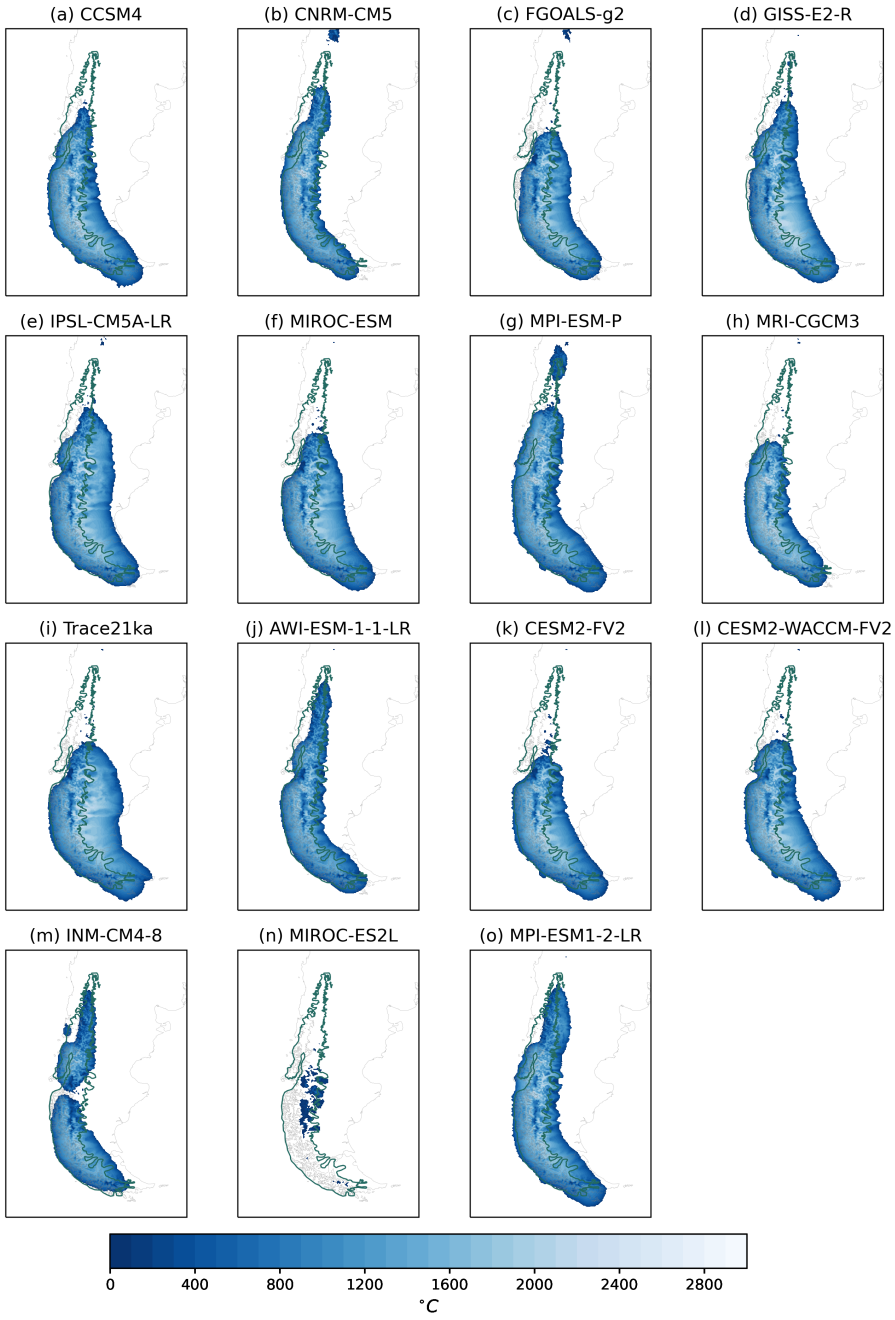

Figure 4. Modelled thickness of the PIS (m). The green line shows the reconstructed glacier extent from the empirical evidence at 20 ka (Davies et al., 2020). The present-day coastline is shown for reference.

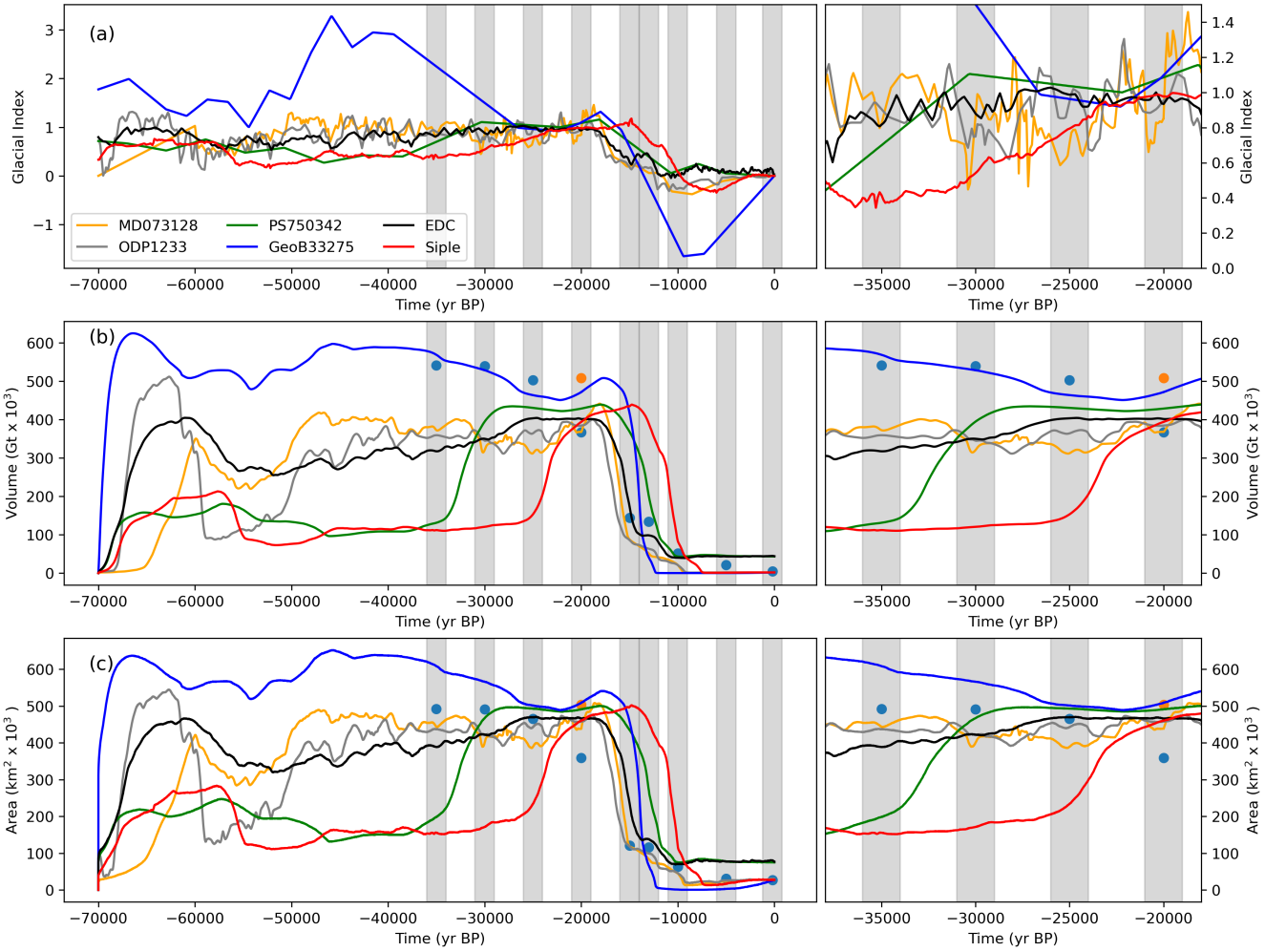

Figure 5. Time series of the glacial indexes used in this study. Modelled ice volumes and glaciated area using MPI-ESM1-2-LR combined with the different cores used in this study (Tab. 3).

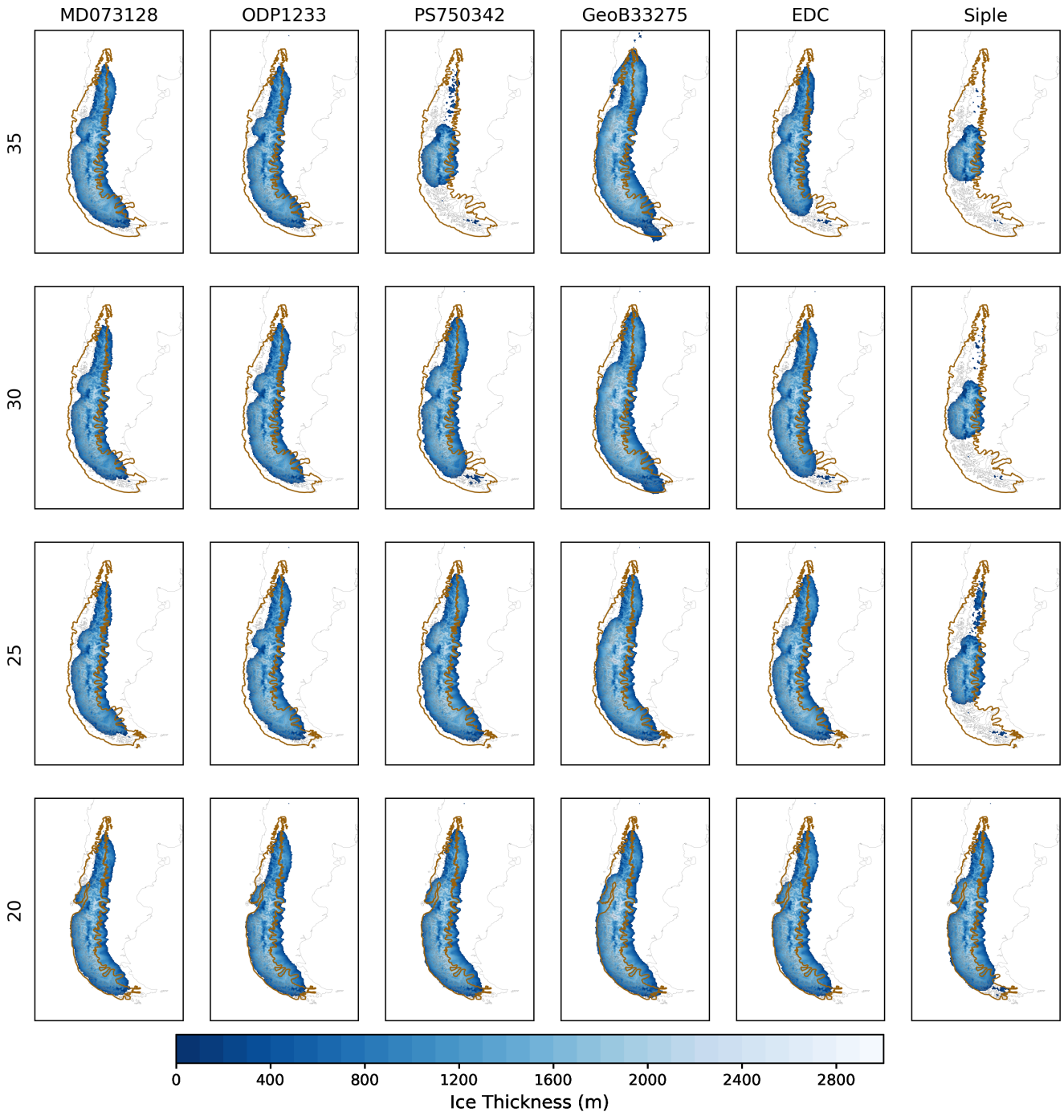

Figure 6. Modelled thickness of the PIS (m) and ice base velocity streamlines for the LGM forced by the different cores used in this study. The green line shows the reconstructed glacier extent from the empirical evidence at 20 ka (Davies et al., 2020). The present-day coastline is shown for reference.

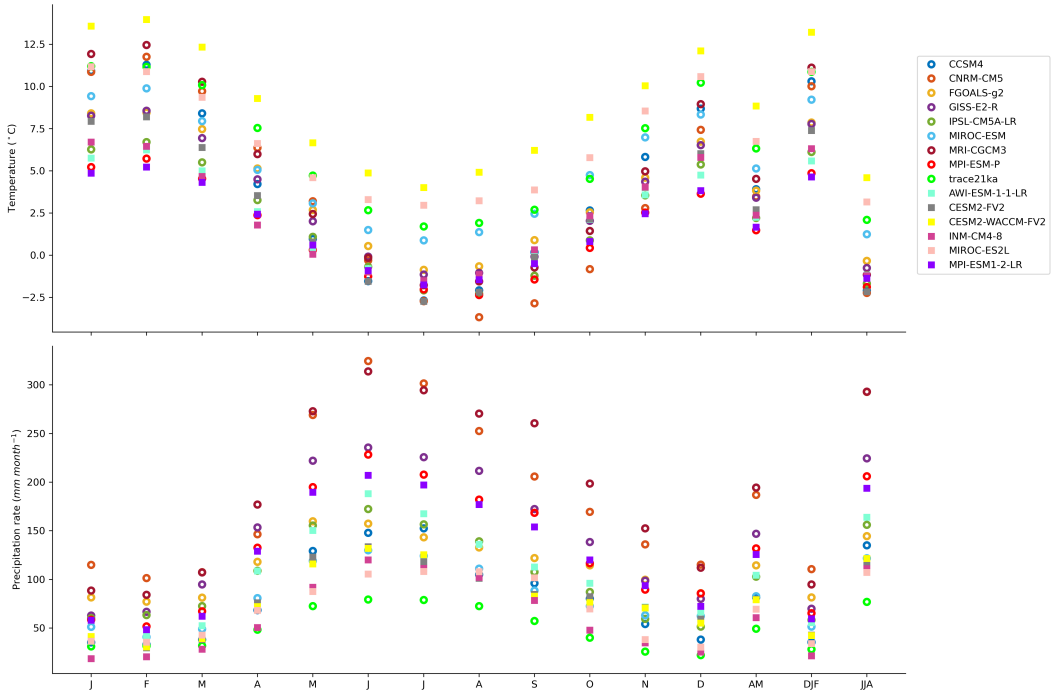

Figure 7. LGM temperatures (upper panel) and precipitation (bottom panel) for the monthly output of CMIP5-PMIP3 and CMIP6-PMIP4 calculated of the northernmost sector of the former PIS. Calculations are made over the grid points that match the reconstructed PIS extents by Davies et al. (2020) within the 38-44° S study zone.

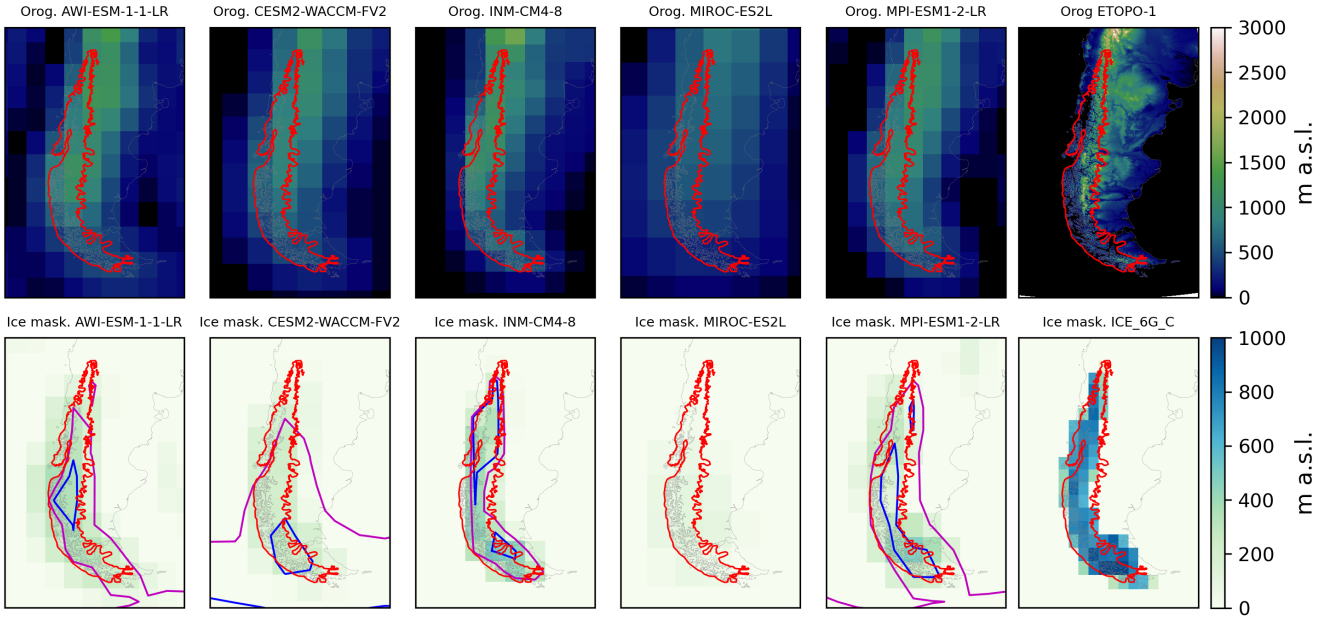

Figure 8. Prescribed topography (upper panel) and ice thickness (bottom panel) the PMIP4 models considered in this study. Etopo-1 (Amante and Eakins, 2009) and the ICE-6G_C reconstruction (Peltier et al., 2015) included as of the ice sheet forcings in PMIP4. The Red line shows the PIS extension for 20 ka (Davies et al., 2020). Blue and purple lines show the isotherm 0 $^{\circ}$C for summer and the annual mean, respectively. Present-day ocean-continent limits are shown for interpretation.

Table 1. Most important parameters in the model set-up. (*) For transient simulations, the Specmap sea-level reconstruction has been used.

Description	Value	Units
Ice density	910.00	$\mathrm{kg\ m^{-3}}$
Gravity acceleration	9.81	$\mathrm{m\ s^{-2}}$
Glen's flow law exponent	3.00	-
Ice specific heat capacity	4170.00	$\mathrm{J\ kg^{-1}\ K^{-1}}$
Ice thermal conductivity	2.10	$\mathrm{J\ kg^{-1}\ K^{-1}}$
Water latent heat of fusion	3.34×10^5	$\mathrm{J\ kg^{-1}\ K^{-1}}$
Asthenosphere density	3300	$\mathrm{kg/m^3}$
Enhancement factor for the SIA and SSA	1, 0.5	-
Geothermal heat flux	100.00	$\mathrm{mW\ m^{-2}}$
Lithosphere density	3300.00	$\mathrm{kg\ m^{-3}}$
Sea level	-120.00 (*)	m
PDD standard deviation	3	°C
Temperature of snow precipitation	0	°C
Temperature of rain precipitation	2	°C
Degree day factor for snow	6	$\mathrm{mm\ d^{-1}\ °C^{-1}}$
Degree day factor for ice	3	$\mathrm{mm\ d^{-1}\ °C^{-1}}$

Table 2. Climate models analysed in the present study.

Model name	PMIP phase	Atmospheric model resolution (°)
CCSM4	III	1.25 x 0.9
CNRM-CM5	III	1.4 x 1.4
FGOALS-g2	III	2.8 x 3-6
GISS-E2-R	III	2.5 x 2.0
IPSL-CM5A-LR	III	3.8 x 1.9
MIROC-ESM	III	2.8 x 2.8
MPI-ESM-P	III	1.88 x 1.9
MRI-CGCM3	III	1.18 x 1.1
Trace21	-	3.7 x 3.7
AWI-ESM-1-1-LR	IV	1.88 x 1.88
CESM-FV2	IV	$\sim$ 2.0 x $\sim$ 2.0
CESM-WACCM-FV2	IV	$\sim$ 2.0 x $\sim$ 2.0
INM-CM4	IV	1.5 x 2.0
MIROC-ES2L	IV	2.8 x 2.8
MPI-ESM1-2-LR	IV	1.88 x 1.88

Table 3. Core records used for the glacial indexes.

Core name	Latitude	Longitude	Proxy
EDC	75.10ºS	123.35ºW	d18O
Siple Dome	81.64ºS	148.77ºW	d18O
ODP-1233	41.00ºS	74.45ºW	UK'37
MD07-3128	52.69ºS	74.56ºW	UK'37
GeoB3327-5	43.24ºS	79.99ºW	UK'37
PS75/034-2	54.37ºS	80.09ºW	UK'37

Code and data availability. SICOPOLIS is a free and open-source software, which can be found at http://sicopolis.net (last access 8th of June, 2023). All simulations in this study were run using SICOPOLIS version 5.2. The PMIP output used in this study can be found on the Earth System Grid Federation website, in particular, CMIP5-PMIP3 (https://esgf-node.ipsl.upmc.fr/search/cmip5-ipsl) and CMIP6-PMIP4 (https://esgf-node.ipsl.upmc.fr/search/cmip6-ipsl). Data will be available once the manuscript has been accepted for publication through zenodo repository

Author contributions. ACL and FRR have contributed equally to this work. The original concept has been conceived by FRR under the supervision of IR and has been further developed by ACL, again under the supervision of IR, with inputs from all authors. All authors contributed to the writing process.

Competing interests. At least one of the (co-)authors is a member of the editorial board of Climate of the Past.

Acknowledgements. ACL acknowledges support from the Agencia Nacional de Investigacion y Desarrollo (ANID) Programa Becas de Doctorado en el Extranjero, Becas Chile for the doctoral scholarship. FRR acknowledges support from the "FONDAP 15110009" Centro de Ciencia del Clima y la Resiliencia (CR)2 (DGF-UChile) and the Ministerio de Educación, Fortalecimiento de la Investigación en Cambio Climático y Conservación Antártica y Subantártica (IES20992). This article is partially based on FRR's undergraduate thesis at the University of Concepcion under IR's and MJC's supervision.

References

Abe-Ouchi, A., Saito, F., Kageyama, M., Braconnot, P., Harrison, S. P., Lambeck, K., Otto-Bliesner, B. L., Peltier, W., Tarasov, L., Peterschmitt, J.-Y., et al.: Ice-sheet configuration in the CMIP5/PMIP3 Last Glacial Maximum experiments, Geoscientific Model Development, 8, 3621–3637, https://doi.org/10.5194/gmd-8-3621-2015, 2015.

Almazroui, M., Ashfaq, M., Islam, M. N., Rashid, I. U., Kamil, S., Abid, M. A., O'Brien, E., Ismail, M., Reboita, M. S., Sörensson, A. A., et al.: Assessment of CMIP6 performance and projected temperature and precipitation changes over South America, Earth Systems and Environment, 5, 155–183, https://doi.org/10.1007/s41748-021-00233-6, 2021.

Amante, C. and Eakins, B. W.: ETOPO1 arc-minute global relief model: procedures, data sources and analysis, NOAA Technical Memorandum NESDIS NGDC-24, https://doi.org/10.7289/V5C8276M, 2009.

Annan, J. and Hargreaves, J. C.: A new global reconstruction of temperature changes at the Last Glacial Maximum, Climate of the Past, 9, 367–376, https://doi.org/10.5194/cp-9-367-2013, 2013.

Bakker, P., Rogozhina, I., Merkel, U., and Prange, M.: Hypersensitivity of glacial summer temperatures in Siberia, Climate of the Past, 16, 371–386, https://doi.org/10.5194/cp-16-371-2020, 2020.

Bartlein, P. J., Harrison, S., Brewer, S., Connor, S., Davis, B., Gajewski, K., Guiot, J., Harrison-Prentice, T., Henderson, A., Peyron, O., et al.: Pollen-based continental climate reconstructions at 6 and 21 ka: a global synthesis, Climate Dynamics, 37, 775–802, https://doi.org/10.1007/s00382-010-0904-1, 2011.

Batchelor, C. L., Margold, M., Krapp, M., Murton, D. K., Dalton, A. S., Gibbard, P. L., Stokes, C. R., Murton, J. B., and Manica, A.: The configuration of Northern Hemisphere ice sheets through the Quaternary, Nature communications, 10, 3713, https://doi.org/10.1038/s41467-019-11601-2, 2019.

Beghin, P., Charbit, S., Dumas, C., Kageyama, M., and Ritz, C.: How might the North American ice sheet influence the northwestern Eurasian climate?, Climate of the Past, 11, 1467–1490, https://doi.org/10.5194/cp-11-1467-2015, 2015.

Berman, A. L., Silvestri, G. E., and Tonello, M. S.: Differences between Last Glacial Maximum and present-day temperature and precipitation in southern South America, Quaternary Science Reviews, 150, 221–233, https://doi.org/10.1016/j.quascirev.2016.08.025, 2016.

Bernales, J., Rogozhina, I., Greve, R., and Thomas, M.: Comparison of hybrid schemes for the combination of shallow approximations in numerical simulations of the Antarctic Ice Sheet, The Cryosphere, 11, 247–265, https://doi.org/10.5194/tc-11-247-2017, 2017.

Boex, J., Fogwill, C., Harrison, S., Glasser, N., Hein, A., Schnabel, C., and Xu, S.: Rapid thinning of the late Pleistocene Patagonian Ice Sheet followed migration of the Southern Westerlies, Scientific Reports, 3, 1–6, https://doi.org/10.1038/srep02118, 2013.

Bown, F., Rivera, A., Pętlicki, M., Bravo, C., Oberreuter, J., and Moffat, C.: Recent ice dynamics and mass balance of Jorge Montt Glacier, Southern Patagonia Icefield, Journal of Glaciology, 65, 732–744, https://doi.org/10.1017/jog.2019.47, 2019.

Bozkurt, D., Rojas, M., Boisier, J. P., Rondanelli, R., Garreaud, R., and Gallardo, L.: Dynamical downscaling over the complex terrain of southwest South America: present climate conditions and added value analysis, Climate Dynamics, 53, 6745–6767, https://doi.org/10.1007/s00382-019-04959-y, 2019.

Braconnot, P., Otto-Bliesner, B., Harrison, S., Joussaume, S., Peterchmitt, J.-Y., Abe-Ouchi, A., Crucifix, M., Driesschaert, E., Fichefet, T., Hewitt, C., et al.: Results of PMIP2 coupled simulations of the Mid-Holocene and Last Glacial Maximum–Part 1: experiments and large-scale features, Climate of the Past, 3, 261–277, https://doi.org/10.5194/cp-3-261-2007, 2007.

Braconnot, P., Harrison, S. P., Kageyama, M., Bartlein, P. J., Masson-Delmotte, V., Abe-Ouchi, A., Otto-Bliesner, B., and Zhao, Y.: Evaluation of climate models using palaeoclimatic data, Nature Climate Change, 2, 417–424, https://doi.org/10.1038/nclimate1456, 2012.

Brook, E. J. and Buizert, C.: Antarctic and global climate history viewed from ice cores, Nature, 558, 200–208, https://doi.org/10.1038/s41586-018-0172-5, 2018.

Bueler, E. and Brown, J.: Shallow shelf approximation as a "sliding law" in a thermomechanically coupled ice sheet model, Journal of Geophysical Research: Earth Surface, 114, 2009.

Calov, R. and Greve, R.: A semi-analytical solution for the positive degree-day model with stochastic temperature variations, Journal of Glaciology, 51, 173–175, https://doi.org/10.3189/172756505781829601, 2005.

Cuzzone, J., Romero, M., and Marcott, S.: Modeling the timing of Patagonian Ice Sheet retreat in the Chilean Lake District from 23–10 ka, The Cryosphere Discussions, 2023, 1–26, https://doi.org/10.5194/tc-2023-68, 2023.

Darvill, C. M., Bentley, M. J., Stokes, C. R., Hein, A. S., and Rodés, Á.: Extensive MIS 3 glaciation in southernmost Patagonia revealed by cosmogenic nuclide dating of outwash sediments, Earth and Planetary Science Letters, 429, 157–169, https://doi.org/10.1016/j.epsl.2015.07.030, 2015.

Darvill, C. M., Bentley, M. J., Stokes, C. R., and Shulmeister, J.: The timing and cause of glacial advances in the southern mid-latitudes during the last glacial cycle based on a synthesis of exposure ages from Patagonia and New Zealand, Quaternary Science Reviews, 149, 200–214, https://doi.org/10.1016/j.quascirev.2016.07.024, 2016.

Davies, B. J., Darvill, C. M., Lovell, H., Bendle, J. M., Dowdeswell, J. A., Fabel, D., García, J.-L., Geiger, A., Glasser, N. F., Gheorghiu, D. M., et al.: The evolution of the Patagonian Ice Sheet from 35 ka to the present day (PATICE), Earth-Science Reviews, 204, 103 152, https://doi.org/10.1016/j.earscirev.2020.103152, 2020.

Denton, G. H., Heusser, C., Lowel, T., Moreno, P. I., Andersen, B. G., Heusser, L. E., Schlühter, C., and Marchant, D. R.: Inter-hemispheric linkage of paleoclimate during the last glaciation, Geografiska Annaler: Series A, Physical Geography, 81, 107–153, https://doi.org/10.1111/1468-0459.00055, 1999.

Doughty, A. M., Schaefer, J. M., Putnam, A. E., Denton, G. H., Kaplan, M. R., Barrell, D. J., Andersen, B. G., Kelley, S. E., Finkel, R. C., and Schwartz, R.: Mismatch of glacier extent and summer insolation in Southern Hemisphere mid-latitudes, Geology, 43, 407–410, https://doi.org/10.1130/G36477.1, 2015.

Evans, M. N., Tolwinski-Ward, S. E., Thompson, D. M., and Anchukaitis, K. J.: Applications of proxy system modeling in high resolution paleoclimatology, Quaternary science reviews, 76, 16–28, https://doi.org/10.1016/j.quascirev.2013.05.024, 2013.

Fernández, A. and Mark, B. G.: Modeling modern glacier response to climate changes along the A ndes C ordillera: A multiscale review, Journal of Advances in Modeling Earth Systems, 8, 467–495, https://doi.org/10.1002/2015MS000482, 2016.

Golledge, N. R., Fogwill, C. J., Mackintosh, A. N., and Buckley, K. M.: Dynamics of the last glacial maximum Antarctic ice-sheet and its response to ocean forcing, Proceedings of the National Academy of Sciences, 109, 16 052–16 056, https://doi.org/10.1073/pnas.1205385109, 2012a.

Golledge, N. R., Mackintosh, A. N., Anderson, B. M., Buckley, K. M., Doughty, A. M., Barrell, D. J., Denton, G. H., Vandergoes, M. J., Andersen, B. G., and Schaefer, J. M.: Last Glacial Maximum climate in New Zealand inferred from a modelled Southern Alps icefield, Quaternary Science Reviews, 46, 30–45, https://doi.org/10.1016/j.quascirev.2012.05.004, 2012b.

Gowan, E. J., Zhang, X., Khosravi, S., Rovere, A., Stocchi, P., Hughes, A. L., Gyllencreutz, R., Mangerud, J., Svendsen, J.-I., and Lohmann, G.: A new global ice sheet reconstruction for the past 80 000 years, Nature communications, 12, 1199, https://doi.org/10.1038/s41467-021-21469-w, 2021.

Greve, R.: Application of a polythermal three-dimensional ice sheet model to the Greenland ice sheet: response to steady-state and transient climate scenarios, Journal of Climate, 10, 901–918, https://doi.org/10.1175/1520-0442(1997)010<0901:AOAPTD>2.0.CO;2, 1997.

Greve, R. and Blatter, H.: Dynamics of ice sheets and glaciers, Springer Science & Business Media, https://doi.org/10.1007/978-3-642-03415-2, 2009.

Hamza, V. M. and Vieira, F.: Global heat flow: new estimates using digital maps and GIS techniques, International Journal of Terrestrial Heat Flow and Applied Geothermics, 1, 6–13, https://doi.org/10.31214/ijthfa.v1i1.6, 2018.

Harrison, S. P., Bartlein, P., Izumi, K., Li, G., Annan, J., Hargreaves, J., Braconnot, P., and Kageyama, M.: Evaluation of CMIP5 palaeo-simulations to improve climate projections, Nature Climate Change, 5, 735–743, https://doi.org/10.1038/nclimate2649, 2015.

Hodgson, D. A., Roberts, S. J., Izagirre, E., Perren, B. B., De Vleeschouwer, F., Davies, S. J., Bishop, T., McCulloch, R. D., and Aravena, J.-C.: Southern limit of the Patagonian Ice Sheet, Quaternary Science Reviews, 321, 108 346, https://doi.org/10.1016/j.quascirev.2023.108346, 2023.

Holden, P. B., Edwards, N., Oliver, K., Lenton, T., and Wilkinson, R.: A probabilistic calibration of climate sensitivity and terrestrial carbon change in GENIE-1, Climate Dynamics, 35, 785–806, https://doi.org/10.1007/s00382-009-0630-8, 2010.

Hughes, A. L., Gyllencreutz, R., Lohne, Ø. S., Mangerud, J., and Svendsen, J. I.: The last Eurasian ice sheets–a chronological database and time-slice reconstruction, DATED-1, Boreas, 45, 1–45, https://doi.org/10.1111/bor.12142, 2016.

Hughes, P. D., Gibbard, P. L., and Ehlers, J.: Timing of glaciation during the last glacial cycle: evaluating the concept of a global 'Last Glacial Maximum'(LGM), Earth-Science Reviews, 125, 171–198, https://doi.org/10.1016/j.earscirev.2013.07.003, 2013.

Hulton, N. R., Purves, R., McCulloch, R., Sugden, D. E., and Bentley, M. J.: The last glacial maximum and deglaciation in southern South America, Quaternary Science Reviews, 21, 233–241, https://doi.org/10.1016/S0277-3791(01)00103-2, 2002.

Huybrechts, P.: Sea-level changes at the LGM from ice-dynamic reconstructions of the Greenland and Antarctic ice sheets during the glacial cycles, Quaternary Science Reviews, 21, 203–231, https://doi.org/10.1016/S0277-3791(01)00082-8, 2002.

Ishii, M., Shouji, A., Sugimoto, S., and Matsumoto, T.: Objective analyses of sea-surface temperature and marine meteorological variables for the 20th century using ICOADS and the Kobe collection, International Journal of Climatology: A Journal of the Royal Meteorological Society, 25, 865–879, https://doi.org/https://doi.org/10.1002/joc.1169, 2005.

Izumi, K., Valdes, P., Ivanovic, R., and Gregoire, L.: Impacts of the PMIP4 ice sheets on Northern Hemisphere climate during the last glacial period, Climate Dynamics, 60, 2481–2499, https://doi.org/10.1007/s00382-022-06456-1, 2023.

Joussaume, S. and Taylor, K.: Status of the paleoclimate modeling intercomparison project (PMIP), World Meteorological Organization-Publications-WMO TD, pp. 425–430, 1995.

Kageyama, M., Albani, S., Braconnot, P., Harrison, S. P., Hopcroft, P. O., Ivanovic, R. F., Lambert, F., Marti, O., Peltier, W. R., Peterschmitt, J.-Y., et al.: The PMIP4 contribution to CMIP6–Part 4: Scientific objectives and experimental design of the PMIP4-CMIP6 Last Glacial Maximum experiments and PMIP4 sensitivity experiments, Geoscientific Model Development, 10, 4035–4055, https://doi.org/10.5194/gmd-10-4035-2017, 2017.

Kageyama, M., Harrison, S. P., Kapsch, M.-L., Lofverstrom, M., Lora, J. M., Mikolajewicz, U., Sherriff-Tadano, S., Vadsaria, T., Abe-Ouchi, A., Bouttes, N., et al.: The PMIP4 Last Glacial Maximum experiments: preliminary results and comparison with the PMIP3 simulations, Climate of the Past, 17, 1065–1089, https://doi.org/10.5194/cp-17-1065-2021, 2021.

Kaplan, M., Coronato, A., Hulton, N., Rabassa, J. O., Kubik, P., and Freeman, S.: Cosmogenic nuclide measurements in southernmost South America and implications for landscape change, Geomorphology, 87, 284–301, https://doi.org/https://doi.org/10.1016/j.geomorph.2006.10.005, 2007.

Kohfeld, K. E., Graham, R. M., De Boer, A. M., Sime, L. C., Wolff, E. W., Le Quéré, C., and Bopp, L.: Southern Hemisphere westerly wind changes during the Last Glacial Maximum: paleo-data synthesis, Quaternary Science Reviews, 68, 76–95, https://doi.org/10.1016/j.quascirev.2013.01.017, 2013.

Lambeck, K., Rouby, H., Purcell, A., Sun, Y., and Sambridge, M.: Sea level and global ice volumes from the Last Glacial Maximum to the Holocene, Proceedings of the National Academy of Sciences, 111, 15 296–15 303, https://doi.org/10.1073/pnas.1411762111, 2014.

Leger, T. P., Hein, A. S., Bingham, R. G., Rodés, Á., Fabel, D., and Smedley, R. K.: Geomorphology and 10Be chronology of the Last Glacial Maximum and deglaciation in northeastern Patagonia, 43° S-71° W, Quaternary Science Reviews, 272, 107 194, https://doi.org/10.1016/j.quascirev.2021.107194, 2021.

Liakka, J., Löfverström, M., and Colleoni, F.: The impact of the North American glacial topography on the evolution of the Eurasian ice sheet over the last glacial cycle, Climate of the Past, 12, 1225–1241, https://doi.org/10.5194/cp-12-1225-2016, 2016.

Lira, M.-P., García, J.-L., Bentley, M. J., Jamieson, S. S., Darvill, C. M., Hein, A. S., Fernández, H., Rodés, Á., Fabel, D., Smedley, R. K., et al.: The Last Glacial Maximum and Deglacial History of the Seno Skyring Ice Lobe (52° S), Southern Patagonia, Frontiers in Earth Science, 10, 892 316, https://doi.org/10.3389/feart.2022.892316, 2022.

Lofverstrom, M. and Liakka, J.: The influence of atmospheric grid resolution in a climate model-forced ice sheet simulation, The Cryosphere, 12, 1499–1510, https://doi.org/10.5194/tc-12-1499-2018, 2018.

Löfverström, M., Caballero, R., Nilsson, J., and Kleman, J.: Evolution of the large-scale atmospheric circulation in response to changing ice sheets over the last glacial cycle, Climate of the Past, 10, 1453–1471, https://doi.org/10.5194/cp-10-1453-2014, 2014.

Marsiat, I.: Simulation of the Northern Hemisphere continental ice sheets over the last glacial-interglacial cycle: experiments with a latitude-longitude vertically integrated ice sheet model coupled to a zonally averaged climate model, 1994.

Mas e Braga, M., Bernales, J., Prange, M., Stroeven, A. P., and Rogozhina, I.: Sensitivity of the Antarctic ice sheets to the warming of marine isotope substage 11c, The Cryosphere, 15, 459–478, https://doi.org/10.5194/tc-15-459-2021, 2021.

Masiokas, M. H., Rabatel, A., Rivera, A., Ruiz, L., Pitte, P., Ceballos, J., Barcaza, G., Soruco, A., Bown, F., Berthier, E., et al.: A review of the current state and recent changes of the Andean cryosphere, Frontiers in Earth Science, 8, 99, https://doi.org/10.3389/feart.2020.00099, 2020.

Meinshausen, M., Smith, S., Calvin, K., Daniel, J., Kainuma, M., Lamarque, J., Matsumoto, K., Montzka, S., Raper, S., Riahi, K., et al.: The paleoclimate modeling intercomparison project contribution to CMIP5, WCRP Coupled Model Intercomparison Project-Phase 5-CMIP5, 16, 15–51, 2011.

Möller, M. and Schneider, C.: Climate sensitivity and mass-balance evolution of Gran Campo Nevado ice cap, southwest Patagonia, Annals of glaciology, 48, 32–42, https://doi.org/10.3189/172756408784700626, 2008.

Monnin, E., Indermuhle, A., Dallenbach, A., Fluckiger, J., Stauffer, B., Stocker, T. F., Raynaud, D., and Barnola, J.-M.: Atmospheric CO2 concentrations over the last glacial termination, science, 291, 112–114, https://doi.org/10.1126/science.291.5501.112, 2001.

Moreno, P. I., Lowell, T. V., Jacobson Jr, G. L., and Denton, G. H.: Abrupt vegetation and climate changes during the last glacial maximum and last termination in the chilean lake district: a case study from canal de la puntilla (41 s), Geografiska Annaler: Series A, Physical Geography, 81, 285–311, https://doi.org/10.1111/1468-0459.00059, 1999.

Moreno, P. I., Denton, G. H., Moreno, H., Lowell, T. V., Putnam, A. E., and Kaplan, M. R.: Radiocarbon chronology of the last glacial maximum and its termination in northwestern Patagonia, Quaternary Science Reviews, 122, 233–249, 2015.

Morlighem, M., Williams, C., Rignot, E., An, L., Bamber, J., Chauche, N., Dowdeswell, J., Dorschel, B., Holland, D., Holland, D., et al.: BedMachine v3: Complete bed topography and ocean bathymetry mapping of Greenland from multi-beam radar sounding combined with mass conservation, https://doi.org/10.1002/2017GL074954, 2017.

Morlighem, M., Rignot, E., Binder, T., Blankenship, D., Drews, R., Eagles, G., Eisen, O., Ferraccioli, F., Forsberg, R., Fretwell, P., et al.: Deep glacial troughs and stabilizing ridges unveiled beneath the margins of the Antarctic ice sheet, Nature Geoscience, 13, 132–137, https://doi.org/10.1038/s41561-019-0510-8, 2020.

Parrenin, F., Masson-Delmotte, V., Köhler, P., Raynaud, D., Paillard, D., Schwander, J., Barbante, C., Landais, A., Wegner, A., and Jouzel, J.: Synchronous change of atmospheric CO2 and Antarctic temperature during the last deglacial warming, Science, 339, 1060–1063, https://doi.org/10.1126/science.1226368, 2013.

Patton, H., Hubbard, A., Andreassen, K., Winsborrow, M., and Stroeven, A. P.: The build-up, configuration, and dynamical sensitivity of the Eurasian ice-sheet complex to Late Weichselian climatic and oceanic forcing, Quaternary Science Reviews, 153, 97–121, https://doi.org/10.1016/j.quascirev.2016.10.009, 2016.

Patton, H., Hubbard, A., Andreassen, K., Auriac, A., Whitehouse, P. L., Stroeven, A. P., Shackleton, C., Winsborrow, M., Heyman, J., and Hall, A. M.: Deglaciation of the Eurasian ice sheet complex, Quaternary Science Reviews, 169, 148–172, https://doi.org/10.1016/j.quascirev.2017.05.019, 2017.

Peano, D., Colleoni, F., Quiquet, A., and Masina, S.: Ice flux evolution in fast flowing areas of the Greenland ice sheet over the 20th and 21st centuries, Journal of Glaciology, 63, 499–513, https://doi.org/10.1017/jog.2017.12, 2017.

Peltier, C., Kaplan, M. R., Birkel, S. D., Soteres, R. L., Sagredo, E. A., Aravena, J. C., Araos, J., Moreno, P. I., Schwartz, R., and Schaefer, J. M.: The large MIS 4 and long MIS 2 glacier maxima on the southern tip of South America, Quaternary Science Reviews, 262, 106 858, https://doi.org/10.1016/j.quascirev.2021.106858, 2021.

Peltier, C., Kaplan, M. R., Sagredo, E. A., Moreno, P. I., Araos, J., Birkel, S. D., Villa-Martínez, R., Schwartz, R., Reynhout, S. A., and Schaefer, J. M.: The last two glacial cycles in central Patagonia: A precise record from the Ñirehuao glacier lobe, Quaternary Science Reviews, 304, 107 873, 2023.

Peltier, W. R., Argus, D., and Drummond, R.: Space geodesy constrains ice age terminal deglaciation: The global ICE-6G_C (VM5a) model, Journal of Geophysical Research: Solid Earth, 120, 450–487, https://doi.org/10.1002/2014JB011176, 2015.

Rogozhina, I., Martinec, Z., Hagedoorn, J., Thomas, M., and Fleming, K.: On the long-term memory of the Greenland Ice Sheet, Journal of Geophysical Research: Earth Surface, 116, https://doi.org/10.1029/2010JF001787, 2011.

Rother, H., Fink, D., Shulmeister, J., Mifsud, C., Evans, M., and Pugh, J.: The early rise and late demise of New Zealand's last glacial maximum, Proceedings of the National Academy of Sciences, 111, 11 630–11 635, https://doi.org/10.1073/pnas.1401547111, 2014.

Sato, T. and Greve, R.: Sensitivity experiments for the Antarctic ice sheet with varied sub-ice-shelf melting rates, Annals of Glaciology, 53, 221–228, https://doi.org/10.3189/2012AoG60A042, 2012.

Sauter, T.: Revisiting extreme precipitation amounts over southern South America and implications for the Patagonian Icefields, Hydrology and Earth System Sciences, 24, 2003–2016, 2020.

Schneider von Deimling, T., Ganopolski, A., Held, H., and Rahmstorf, S.: How cold was the last glacial maximum?, Geophysical Research Letters, 33, https://doi.org/10.1029/2006GL026484, 2006.

Seroussi, H., Nowicki, S., Payne, A. J., Goelzer, H., Lipscomb, W. H., Abe-Ouchi, A., Agosta, C., Albrecht, T., Asay-Davis, X., Barthel, A., et al.: ISMIP6 Antarctica: a multi-model ensemble of the Antarctic ice sheet evolution over the 21st century, The Cryosphere, 14, 3033–3070, https://doi.org/10.5194/tc-14-3033-2020, 2020.

Shulmeister, J., Thackray, G. D., Rittenour, T. M., Fink, D., and Patton, N. R.: The timing and nature of the last glacial cycle in New Zealand, Quaternary Science Reviews, 206, 1–20, https://doi.org/https://doi.org/10.1016/j.quascirev.2018.12.020, 2019.

Simms, A. R., Lisiecki, L., Gebbie, G., Whitehouse, P. L., and Clark, J. F.: Balancing the last glacial maximum (LGM) sea-level budget, Quaternary Science Reviews, 205, 143–153, https://doi.org/10.1016/j.quascirev.2018.12.018, 2019.

Stokes, C. R.: Deglaciation of the Laurentide Ice Sheet from the Last Glacial Maximum., Cuadernos de investigación geográfica., 43, 377–428, https://doi.org/10.18172/cig.3237, 2017.

Tarasov, L., Dyke, A. S., Neal, R. M., and Peltier, W. R.: A data-calibrated distribution of deglacial chronologies for the North American ice complex from glaciological modeling, Earth and Planetary Science Letters, 315, 30–40, https://doi.org/10.1016/j.epsl.2011.09.010, 2012.

Tierney, J. E., Zhu, J., King, J., Malevich, S. B., Hakim, G. J., and Poulsen, C. J.: Glacial cooling and climate sensitivity revisited, Nature, 584, 569–573, https://doi.org/10.1038/s41586-020-2617-x, 2020.

Troch, M., Bertrand, S., Lange, C. B., Cárdenas, P., Arz, H., Pantoja-Gutiérrez, S., De Pol-Holz, R., and Kilian, R.: Glacial isostatic adjustment near the center of the former Patagonian Ice Sheet (48° S) during the last 16.5 kyr, Quaternary Science Reviews, 277, 107 346, https://doi.org/10.1016/j.quascirev.2021.107346, 2022.

Ullman, D., LeGrande, A., Carlson, A. E., Anslow, F., and Licciardi, J.: Assessing the impact of Laurentide Ice Sheet topography on glacial climate, Climate of the Past, 10, 487–507, https://doi.org/10.5194/cp-10-487-2014, 2014.

Wolff, I. W., Glasser, N. F., Harrison, S., Wood, J. L., and Hubbard, A.: A steady-state model reconstruction of the patagonian ice sheet during the last glacial maximum, Quaternary Science Advances, 12, 100 103, https://doi.org/10.1016/j.qsa.2023.100103, 2023.

Yan, Q., Wei, T., and Zhang, Z.: Modeling the climate sensitivity of Patagonian glaciers and their responses to climatic change during the global last glacial maximum, Quaternary Science Reviews, 288, 107 582, https://doi.org/10.1016/j.quascirev.2022.107582, 2022.

Zech, R., Zech, J., Kull, C., Kubik, P. W., and Veit, H.: Early last glacial maximum in the southern Central Andes reveals northward shift of the westerlies at˜ 39 ka, Climate of the Past, 7, 41–46, https://doi.org/10.5194/cp-7-41-201, 2011.